The Astrophysical Journal, 681:1505–1523, 2008 July 10

Fe AND Al ABUNDANCES FOR 180 RED GIANTS IN THE GLOBULAR CLUSTER OMEGA CENTAURI (NGC 5139)

Christian I. Johnson,[1] Catherine A. Pilachowski,[1] Jennifer Simmerer,[2] and Dustin Schwenk[3]

Received 2008 February 8; accepted 2008 March 24

ABSTRACT

We present radial velocities and Fe and Al abundances for 180 red giant branch (RGB) stars in the Galactic globular cluster Omega Centauri (ω Cen). The majority of our data lie in the range $11.0 < V < 13.5$, which covers the RGB from about 1 mag above the horizontal branch to the RGB tip. The selection procedures are biased toward preferentially observing the more metal-poor and luminous stars of ω Cen. Abundances were determined using equivalent width measurements and spectrum synthesis analyses of moderate resolution spectra ($R \approx 13{,}000$) obtained with the Blanco 4 m telescope and Hydra multifiber spectrograph. Our results are in agreement with previous studies as we find at least four different metallicity populations with $[\mathrm{Fe/H}] = -1.75, -1.45, -1.05$, and -0.75, with a full range of $-2.20 \lesssim [\mathrm{Fe/H}] \lesssim -0.70$. [Al/Fe] ratios exhibit large star-to-star scatter for all populations, with the more than 1.0 dex range of [Al/Fe] decreasing for stars more metal-rich than $[\mathrm{Fe/H}] \sim -1.4$. The minimum [Al/Fe] abundance observed for all metallicity populations is $[\mathrm{Al/Fe}] \sim +0.15$. The maximum abundance of $\log \epsilon(\mathrm{Al})$ is reached for stars with $[\mathrm{Fe/H}] \sim -1.4$ and does not increase further with stellar metallicity. We interpret these results as evidence for Type II SNe providing the minimum [Al/Fe] ratio and a mass spectrum of intermediate-mass asymptotic giant branch stars causing the majority of the [Al/Fe] scatter. These results seem to fit in the adopted scheme that star formation occurred in ω Cen over >1 Gyr.

Subject headings: globular clusters: general — globular clusters: individual (ω Centauri, NGC 5139) — stars: abundances — stars: Population II

Online material: color figures, machine-readable tables

1. INTRODUCTION

The Galactic globular cluster Omega Centauri (ω Cen) presents a unique opportunity to study the chemical evolution of both a small stellar system and stars with common formation histories covering a metallicity range of more than a factor of 10, a defining characteristic of ω Cen that has been known since the initial discovery of its unusually broad red giant branch (RGB) by Woolley (1966). Although ω Cen is the most massive Galactic globular cluster, with an estimated mass of $\sim(2\text{–}7) \times 10^6\ M_\odot$ (Richer et al. 1991; Meylan et al. 1995; van de Ven et al. 2006), it does not appear to have an exceptionally deep gravitational potential well (Gnedin et al. 2002). This seems to negate a simple explanation that ω Cen evolved as a typical globular cluster that was more easily able to retain supernova (SN) and asymptotic giant branch (AGB) ejecta for self-enrichment. This fact coupled with the cluster's retrograde orbit and disk crossing time of $\sim(1\text{–}2) \times 10^8$ yr (e.g., Dinescu et al. 1999), which could severely inhibit star formation, are some of the strongest arguments against ω Cen having a Galactic origin. Instead, it has been proposed (e.g., Dinescu et al. 1999; Smith et al. 2000; Gnedin et al. 2002; Bekki & Norris 2006) that ω Cen may be the remaining nucleus of a dwarf spheroidal galaxy that evolved in isolation and was later accreted by the Milky Way, suggesting the progenitor system was perhaps a factor of 100–1000 times more massive than what is presently observed.

Recent spectroscopic and photometric studies (Norris & Da Costa 1995; Norris et al. 1996; Suntzeff & Kraft 1996; Lee et al. 1999; Hilker & Richtler 2000; Hughes & Wallerstein 2000; Pancino et al. 2000; Smith et al. 2000; van Leeuwen et al. 2000; Rey et al. 2004; Stanford et al. 2004, 2006, 2007; Piotto et al. 2005; Sollima et al. 2005a, 2005b, 2006; Kayser et al. 2006; van Loon et al. 2007; Villanova et al. 2007) have confirmed the existence of up to five separate stellar populations ranging in metallicity from $[\mathrm{Fe/H}] \sim -2.2$ to -0.5, with a peak in the metallicity distribution near $[\mathrm{Fe/H}] \sim -1.7$ and a long tail extending to higher metallicities. In addition to the metal-poor and intermediate-metallicity populations initially seen in the Woolley (1966) photometric study, Lee et al. (1999) and Pancino et al. (2000) discovered the existence of the most metal-rich RGB at $[\mathrm{Fe/H}] \sim -0.5$, commonly referred to as the anomalous RGB (RGB-a). The RGB-a is primarily observed in the central region of the cluster and contains approximately 5% of the total stellar population (Pancino et al. 2000), in contrast to the dominant metal-poor population that contains roughly 75% of cluster stars. In addition, there is some evidence (Norris et al. 1997) that the metal-rich population exhibits smaller radial velocity dispersion and rotation than the metal-poor population. Sollima et al. (2005b) confirmed the Norris et al. (1997) results but also showed that the most metal-rich stars ($[\mathrm{Fe/H}] > -1$) exhibit an increasing velocity dispersion as a function of increasing metallicity, which could be evidence for accretion events occurring within ω Cen's progenitor system (Ferraro et al. 2002; Pancino et al. 2003); however, this result is not yet confirmed (Platais et al. 2003, but see also Hughes et al. 2004). It should be noted that Pancino et al. (2007), using radial velocity measurements of 650 members with measurement uncertainties of order 0.5 km s^{-1}, have found no evidence for rotational differences among the different metallicity groups.

The distribution of main-sequence turnoff (MSTO) and subgiant branch (SGB) stars matches that observed on the RGB, such that one can trace the evolutionary sequence of each population

[1] Department of Astronomy, Indiana University, Swain West 319, 727 East Third Street, Bloomington, IN 47405-7105; cijohnson@astro.indiana.edu; catyp@astro.indiana.edu.

[2] Lund Observatory, Box 43, SE 221-00 Lund, Sweden; jennifer@astro.lu.se.

[3] Department of Physics, University of Illinois at Urbana-Champaign, 2910 Artesia Crossing, Urbana, IL 61802; schwenk@uiuc.edu.

from at least the MSTO to the RGB using high-precision photometry (e.g., Villanova et al. 2007). The main sequence (MS) has proved to be as complex as the SGB and RGB, with the discovery by Anderson (1997) of a red and blue MS (BMS). Interestingly, Piotto et al. (2005) discovered that the BMS was more metal-rich than the red MS, suggesting the BMS could be explained assuming a higher He content, perhaps as high as $Y \sim 0.38$ (Bedin et al. 2004; Norris 2004; Lee et al. 2005; Piotto et al. 2005).

While it is clear that multiple populations are present in this cluster, there has been some debate regarding the age of each population. There is general agreement that the age range is between about 0 and 6 Gyr (Norris & Da Costa 1995; Hilker & Richtler 2000; Hughes & Wallerstein 2000; Pancino et al. 2002; Origlia et al. 2003; Ferraro et al. 2004; Hilker et al. 2004; Rey et al. 2004; Sollima et al. 2005a, 2005b; Villanova et al. 2007), although the recent work by Stanford et al. (2006) suggests the most likely age range is ~2–4 Gyr, with the metal-rich stars being younger. For the case of monotonic chemical enrichment in a single system, one would expect the more metal-rich stars to be younger than the more metal-poor; however, this assumption has been questioned by Villanova et al. (2007), who suggested the metal-rich stars and 33% of the metal-poor stars are the oldest with the remaining two-thirds of the metal-poor population being 3–4 Gyr younger. The picture of ω Cen's formation is further compounded by observations of RR Lyrae horizontal branch (HB) stars that reveal a bimodal metallicity distribution *without* a trend in He enhancement as a function of [Fe/H] (Sollima et al. 2006). The important point here is that a group of RR Lyrae stars exists with the same metallicity as the BMS but without the presumed He enhancement. A He-rich secondary population would not produce a significant RR Lyrae population unless a $\gtrsim$4 Gyr age difference was present with respect to the dominant metal-poor population (Sollima et al. 2006). The required age difference is therefore inconsistent with most age spread estimates that put $\Delta\tau \lesssim 4$ Gyr.

The chemical evolution history of ω Cen has so far proved difficult to interpret from measured abundances of light ($Z \lesssim 27$), α, Fe-peak, *s*-process, and *r*-process elements. In "normal" Galactic globular clusters, C, N, O, F, Na, Mg (sometimes), and Al often exhibit large star-to-star variations, in some cases exceeding more than a factor of 10 (e.g., see recent review by Gratton et al. 2004). In contrast, the heavier α-elements (e.g., Ca and Ti) show little to no variation and are enhanced relative to Fe at $[\alpha/\mathrm{Fe}] \sim +0.30$, with a decreasing ratio for clusters with $[\mathrm{Fe/H}] > -1$. Likewise, Fe and all other Fe-peak, *s*-process, and *r*-process elements show star-to-star variations of ~0.10–0.30 dex. In addition, nearly all globular clusters are enriched in *r*-process relative to *s*-process elements by about 0.20 dex. In ω Cen, [Fe/H] covers a range of more than 1.5 dex and, as previously stated, it has a potential well comparable to that of other globular clusters, suggesting it had to be different in the past to undergo self-enrichment. The scenario of two or more globular clusters merging seems unlikely now given the results of Pancino et al. (2007) and the typically large orbital velocities coupled with the small velocity dispersions of clusters (Ikuta & Arimoto 2000). While ω Cen exhibits large abundance variations for several of the light elements at various metallicities (e.g., Norris & Da Costa 1995; Smith et al. 2000), the mean heavy α-element enhancement is surprisingly uniform at $[\alpha/\mathrm{Fe}] \sim +0.30$ to +0.50 (Norris & Da Costa 1995; Smith et al. 2000; Villanova et al. 2007), with perhaps a trend of decreasing $[\alpha/\mathrm{Fe}]$ at $[\mathrm{Fe/H}] > -1$ (Pancino et al. 2002). The *s*-process elements show a clear increase in abundance relative to Fe with a plateau occurring at $[\mathrm{Fe/H}] \sim -1.40$ to -1.20 (Norris & Da Costa 1995; Smith et al. 2000). However, unlike in globular clusters, *s*-process elements are overabundant with respect to *r*-process elements, where [Ba/Eu] typically reaches between 0.5 and 1.0 (Smith et al. 2000), indicating a strong presence of AGB ejecta.

Many globular cluster giants show clear C-N, O-Na, O-Al, and Mg-Al, and in the case of M4 (Smith et al. 2005), F-Na anticorrelations alongside a Na-Al correlation (e.g., Gratton et al. 2004). In addition to these anomalies being present in the atmospheres of RGB stars, similar relations have been observed in some globular cluster MS and MSTO stars (e.g., Cannon et al. 1998; Gratton et al. 2001; Cohen et al. 2002; Briley et al. 2004a, 2004b; Boesgaard et al. 2005). According to standard evolutionary theory, first dredge-up brings the products of MS core hydrogen burning to the surface and homogenizes approximately 70%–80% of the star, resulting in C depletion, N enhancement, and a lowering of the $^{12}C/^{13}C$ ratio from about 90 to 25 (e.g., Salaris et al. 2002). The decline in [C/Fe] and $^{12}C/^{13}C$ has been verified via observations in both globular cluster (Bell et al. 1979; Carbon et al. 1982; Langer et al. 1986; Bellman et al. 2001) and field stars (Charbonnel & do Nascimento 1998; Gratton et al. 2000; Keller et al. 2001) as strong evidence for in situ mixing occurring along the RGB. However, as the advancing hydrogen-burning shell (HBS) crosses the molecular weight discontinuity left by the convective envelope's deepest point of penetration, extra mixing not predicted by canonical theory occurs in both field and cluster stars, driving down [C/Fe] further and allowing $^{12}C/^{13}C$ to reach the CN-cycle equilibrium value of ~4. The mechanism responsible for this extra mixing is not known, although thermohaline mixing (Charbonnel & Zahn 2007) may ameliorate the problem. While halo field and cluster giants share these same trends, differences arise when considering O, Na, and Al abundances. Field stars do not exhibit most of the familiar correlations/anticorrelations and large star-to-star variations seen in globular cluster stars and instead remain mostly constant from the MS to the RGB tip (e.g., Ryan et al. 1996; Fulbright 2002; Gratton et al. 2000).

The reason for the observed differences between cluster and field giants is not known, but obviously the higher density cluster environment is a key factor. Coupled O depletions and Na/Al enhancements are clear signs of high-temperature ($T \gtrsim 40 \times 10^6$ K) H-burning via the ON, NeNa, and MgAl proton-capture cycles, but this does not necessarily mean those cycles are operating in the RGB stars we presently observe and instead may be from the ejecta of intermediate-mass (IM) AGB stars (~3–8 $M_\odot$) that underwent hot bottom burning (HBB) and polluted the gas from which the current stars formed. One of the strongest arguments against in situ mixing is the observed abundance relations on the MS and MSTO matching those on the RGB because these stars are both too cool for the ON, NeNa, and MgAl cycles to operate and their shallow envelope convection zones do not reach deep enough to bring up even CN-cycled material. In addition, Shetrone (1996) showed that at least in M13 giants, ^{24}Mg is anticorrelated with Al instead of ^{25}Mg and/or ^{26}Mg, which means temperatures not achievable in low-mass RGB stars (at least 70×10^6 K) are needed to activate the full MgAl chain (Langer et al. 1997); however, these temperatures are reached in HBB conditions. Current models of low-mass RGB stars (e.g., Denissenkov & Weiss 2001) indicate ^{27}Al is only produced deep in the stellar interior by burning ^{25}Mg and convective mixing reaching these depths would cause a second increase in the surface abundance of both ^{23}Na and ^{4}He. It should be noted that if it is instead $^{26}Al(\tau_{1/2} \sim 1 \times 10^6$ yr) causing the abundance anomalies on the upper RGB, then the O-Na and Na-Al relations

can be explained in a self-consistent manner via in situ mixing (Denissenkov & Weiss 2001). Also, there is some evidence that O depletions and Na/Al enhancements become stronger in the upper ∼0.7 mag before the RGB tip in M13 (e.g., Sneden et al. 2004; Johnson et al. 2005), indicating the possible operation of additional deep mixing episodes in some stars. Although it is more difficult to believe in situ mixing is responsible for the ^{24}Mg–^{27}Al anticorrelation, the same may not be true for O and Na. In or just above the HBS of a metal-poor low-mass RGB star, the O-Na anticorrelation can be naturally explained because the ON and NeNa cycles can operate at $T \sim 40 \times 10^6$ K (Denisenkov & Denisenkova 1990; Langer et al. 1993). Of course, this cannot be the case for any O-Na anticorrelation observed in MSTO and SGB stars and does require convective mixing in RGB stars to penetrate past the radiative zone separating the bottom of the convective envelope and the top of the HBS.

While pollution from a previous generation of more massive AGB stars seems an attractive explanation, there are a few important issues. Predicted IM-AGB stellar yields are sensitive to the adopted treatment of convection because it affects other important parameters such as luminosity, number of thermal pulses, third dredge-up efficiency, envelope temperature structure, and mass loss (Ventura & D'Antona 2005a). The two most common methods employed are mixing length theory (MLT; e.g., Fenner et al. 2004) and the full spectrum of turbulence (FST) model (e.g., Ventura & D'Antona 2005b), with the latter providing more efficient convection. In ω Cen and all other globular clusters observed, the [C+N+O/Fe] sum is constant (Pilachowski 1988; Dickens et al. 1991; Norris & Da Costa 1995; Smith et al. 1996; Ivans et al. 1999), but models based on MLT indicate stars forming from different generations of AGB ejecta should show a large increase in the CNO sum (e.g., Lattanzio et al. 2004). In contrast, FST models keep [C+N+O/Fe] constant to within about a factor of 2 due to enhanced mass loss and fewer third dredge-up episodes (Ventura & D'Antona 2005b). Although Na and Al production could be due to HBB, it is difficult to produce the observed O depletion of 1.0 to 1.5 dex along with the required Na enhancement (e.g., Denissenkov & Herwig 2003; but see also Ventura & D'Antona 2005b). Self-consistent models of globular cluster enrichment from AGB ejecta fail to reproduce the MgAl anticorrelation seen in several globular clusters, including ω Cen, where Mg increases relative to Al instead of decreases (Fenner et al. 2004). Without an evolutionary scenario, O-deficient, Na/Al-enhanced stars must have preferentially formed out of enriched gas relative to "O-normal" stars (i.e., [O/Fe] ∼ +0.30) and Yong et al. (2003) point out that even with no O present in the enriched gas, these stars would require a composition of 90% enriched, 10% "normal" material to obtain the observed O deficiency. Lastly, AGB stellar envelopes contain roughly 36% He by mass (Lattanzio et al. 2004), but O-poor, Na/Al-rich stars do not appear to be particularly He-rich; however, this does not rule out AGB stars as the source of the He-rich BMS observed in ω Cen. Given the evidence for and against evolutionary and primordial processes, a hybrid scenario probably needs to be invoked to explain all abundance anomalies.

Given the inherently large spread in metallicity of stars in ω Cen and that Al is the heaviest element sensitive to proton-capture nucleosynthesis at temperatures achieved in the interiors of low-mass metal-poor RGB stars, we present radial velocities, Fe, and Al abundances for 180 RGB stars covering $-2.20 < [\mathrm{Fe/H}] < -0.70$. With additional data from the literature covering from the MS to the RGB tip, we address the issues of star formation and possible pollution sources driving the chemical evolution of ω Cen as a function of metallicity.

TABLE 1
Hydra Observations of ω Cen Giants

Hydra Setup	Wavelength (Å)	UT Date	Exposure (s)
1	6600	2003 Jul 17	1 × 1800
2	6600	2003 Jul 18	1 × 1800
2	6600	2003 Jul 18	4 × 2700
3	6600	2003 Jul 19	2 × 2700
3	6600	2003 Jul 19	1 × 3600

2. OBSERVATIONS AND REDUCTIONS

The observations of all 180 giants in ω Cen were obtained with the Blanco 4 m telescope using the Hydra multifiber positioner and bench spectrograph at the Cerro Tololo Inter-American Observatory. All observations were obtained using the "large" 300 μm (2″) fibers. The full spectral coverage ranged from ∼6450–6750 Å, centered on ∼6600 Å; however, wavelengths blueward of ∼6500 Å lie on the shoulder of the filter response curve, making continuum placement difficult. Therefore, we truncated the spectra to include only the region from 6500–6750 Å. The 316 line mm^{-1} echelle grating and Blue Air Schmidt Camera provided a resolving power of $R(\lambda/\Delta\lambda) \approx 13{,}000$ (0.5 Å FWHM) at 6600 Å. A list of our observation dates and exposure times is provided in Table 1.

Target stars, coordinates, photometry, and membership probability were taken from the proper motion study by van Leeuwen et al. (2000). Stars were given priority in the Hydra assignment program based on V magnitude, with a focus on stars in the range $11.0 < V < 14.0$, which includes all giants in the cluster brighter than the HB up to the RGB tip. Only stars with membership probabilities ≳80% were included for possible study. All observations took place between 2003 July 17 and 2003 July 19. Three different Hydra setups were used with exposure times ranging from 1800 to 3600 s. Each setup allowed approximately 100 fibers to be placed on targets, yielding a total initial sample size of nearly 300 stars. At $V \sim 13.5$, reaching a signal-to-noise (S/N) ratio of 100 requires 3 hr of total integration time. Unfortunately, weather and time constraints led to one of the setups receiving less than 2 hr of integration time with an average S/N of less than 50. Many of these stars had to be excluded from analysis due to poor S/N; however, the final sample size still includes nearly 200 stars. These are shown in Figure 1 along with the complete sample given in van Leeuwen et al. (2000) for $11.0 < V < 14.0$.

Due to ω Cen's broad RGB, selection effects must be taken into account when interpreting abundance results. Figure 2 shows our observed completion fraction of RGB stars both as a function of V magnitude and $B - V$ color compared to the deeper photometric study by Rey et al. (2004). Since our observing program is biased toward selecting brighter stars, our sample includes more metal-poor than metal-rich stars because metal-rich stars have lower V magnitudes due to H^- opacity increasing with increasing metallicity. While we observed 75% of all RGB tip stars available, the fraction of stars observed decreases to ∼15%–50% in the range $11.5 < V < 13.0$. Likewise, in considering completeness in $B - V$ color, our sample includes stars of higher luminosity for a given $B - V$, biasing our results toward the more metal-poor regime.

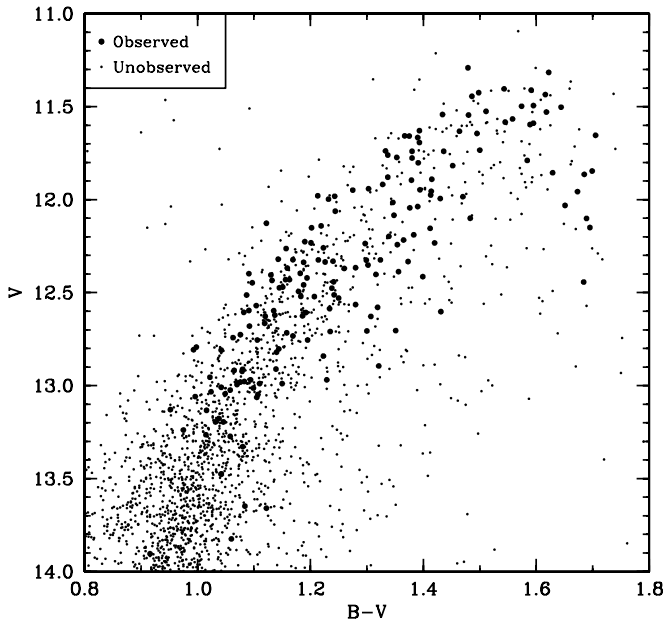

FIG. 1.—Color-magnitude diagram of the upper RGB for ω Cen. The large filled circles indicate program stars and the small filled circles are those available from the van Leeuwen et al. (2000) proper motion study. [*See the electronic edition of the Journal for a color version of this figure.*]

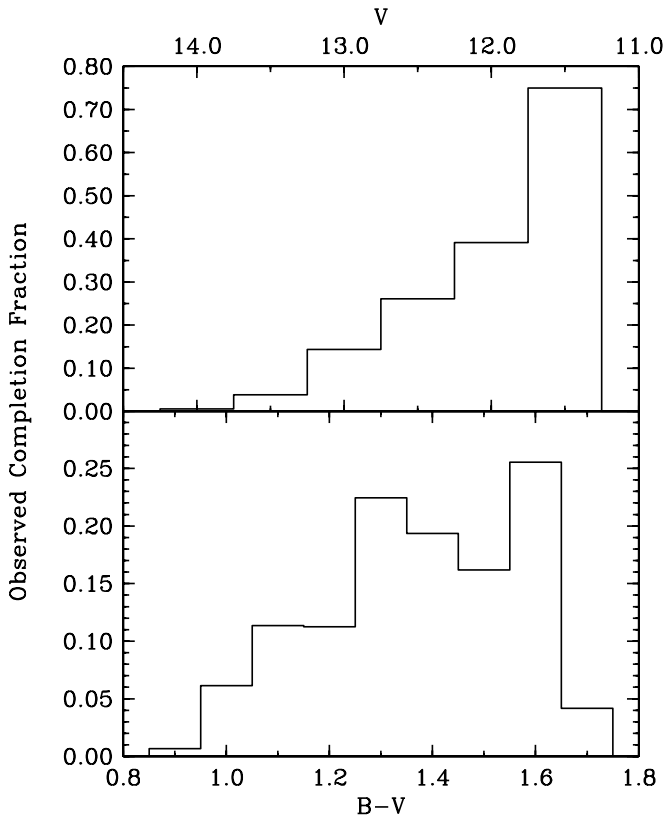

FIG. 2.—Histogram showing the observed completion fraction of this study. The data are compared to the deeper photometric study of Rey et al. (2004). The top panel shows the completion fraction binned by apparent V magnitude with bin sizes of 0.5 mag and the bottom panel shows the completion fraction binned by $B - V$ color in 0.1 mag intervals.

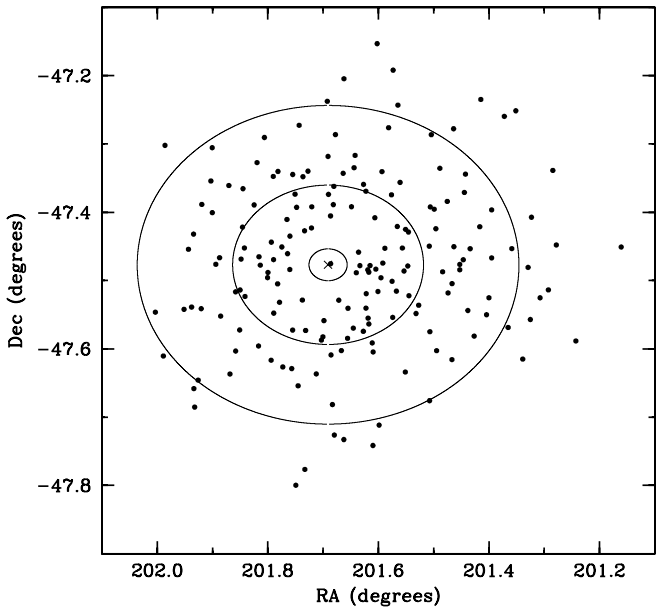

FIG. 3.—Program stars are shown in terms of position in the field. The cross indicates the field center at 201.691°, −47.4769° (J2000.0) ($13^h26^m45.9^s$, −47°28′37.0″). The ellipses indicate 1, 5, and 10 times the core radius of 1.40′. [*See the electronic edition of the Journal for a color version of this figure.*]

Figure 3 shows the location of our observed stars in right ascension and declination relative to the cluster center, defined by van Leeuwen et al. (2000) as $13^h26^m45.9^s$, −47°28′37.0″ (J2000.0) and marked with a cross in the figure. Since some evidence exists for a correlation between metallicity and distance from the cluster center (Norris et al. 1996, 1997; Suntzeff & Kraft 1996; Hilker & Richtler 2000; Pancino et al. 2000; Rey et al. 2004), we have observed stars as uniformly as possible at radii extending out to ∼20′. Near the cluster center, crowding and the physical size of the fibers limited the number of observations inside about 2 core radii, where the core radius is approximately 1.40′ (Harris 1996, rev. 2003 February). We illustrate this effect with the ellipses in Figure 3 that correspond to 1, 5, and 10 core radii.

Basic data reductions were accomplished using the IRAF[4] package `ccdproc` to trim the bias overscan region and apply bias level corrections. The IRAF task `dohydra` was employed to correct for scattered light, extract the one-dimensional spectra, remove cosmic rays, apply a flat-field correction, linearize the wavelength scale, and subtract the sky spectrum. Wavelength calibrations were carried out using a high-S/N solar sky spectrum because the ThAr lamp was unavailable. Standard IRAF tasks were used to co-add and normalize the spectra. Typical S/N ratios for individual exposures ranged from ∼25–50, with co-added spectra having S/N between 75 and 150.

3. RADIAL VELOCITY DETERMINATIONS

The location of ω Cen in the thick disk (Dinescu et al. 1999) makes field star contamination a more serious problem than for typical halo globular clusters. While we initially only chose targets with high membership probabilities from van Leeuwen et al. (2000), direct measurements of target radial velocities assist with membership confirmation. Radial velocities were determined using the IRAF tasks `rvcor`, to correct for heliocentric motion, and

[4] IRAF is distributed by the National Optical Astronomy Observatories, which are operated by the Association of Universities for Research in Astronomy, Inc., under cooperative agreement with the National Science Foundation.

TABLE 2
Radial Velocity and Membership Information

Star[a]	Alt. ID[b]	V_R (km s^{-1})	Error (km s^{-1})	σ from Mean	Membership Probability[c]
9.....	370	211.9	1.8	1.7	99
5009.....	548	230.7	1.6	0.1	100
6017.....	240	248.4	1.6	1.4	98
10012.....	43	236.2	1.6	0.4	98
11019.....	537	238.3	1.7	0.6	99
Cluster Mean Values					
Mean	...	231.8	1.6	0.8	...
Median	...	232.0	1.5	0.6	...
σ	...	11.7	0.3	0.6	...

Note.—Table 2 is published in its entirety in the electronic edition of the *Astrophysical Journal*. A portion is shown here for guidance regarding its form and content.

[a] Identifier from van Leeuwen et al. (2000).

[b] Identifier from Woolley (1966).

[c] Membership probability from van Leeuwen et al. (2000).

fxcor, to determine the heliocentric radial velocity. For the comparison spectrum, we used the same high-S/N daylight sky spectrum that was used for wavelength calibration. A summary of our determined radial velocities along with membership probabilities from van Leeuwen et al. (2000) are given in Table 2.

The largest radial velocity study of ω Cen stars to date is by Reijns et al. (2006), who determined radial velocities for ∼2000 RGB stars. Their study finds a strongly peaked distribution near 232 km s^{-1}, with a median uncertainty of less than 2 km s^{-1} and a velocity dispersion of ∼6 km s^{-1} for the inner 25′ of the cluster. Similarly, Mayor et al. (1997) find $\langle V_R \rangle = 232.8 \pm 0.7$ km s^{-1} ($\sigma \sim 17.5$ km s^{-1}) for 471 stars and Suntzeff & Kraft (1996) find $\langle V_R \rangle = 234.7 \pm 1.3$ km s^{-1} ($\sigma = 11.3$ km s^{-1}) for their "bright" sample of 199 stars. Recently, Pancino et al. (2007) determined radial velocities for 650 RGB stars and found $\langle V_R \rangle = 233.4 \pm 0.5$ km s^{-1} ($\sigma = 13.2$ km s^{-1}). We find in agreement with these studies: $\langle V_R \rangle = 231.8$ km s^{-1} ± 1.6 km s^{-1} ($\sigma = 11.6$ km s^{-1}). Our observations do not provide an absolute velocity calibration, but comparison with the other observations of the average velocity of cluster stars suggests that the systematic error of our radial velocities is less than about 2 km s^{-1}. Since all of our stars listed in Table 2 are less than 3 σ away from the cluster averaged velocity and ω Cen's velocity is high relative to the general field population, it is unlikely any of our targets are field stars.

4. ANALYSIS

We have derived Fe and Al abundances using lines available in the spectral range 6500–6750 Å with either equivalent width or synthetic spectrum analyses. Spectrum synthesis was used to determine Al abundances in metal-rich and/or CN-strong stars. When multiple lines were available, the stated abundances represent the average of the individual lines. Effective temperatures ($T_{\rm eff}$) and gravities ($\log g$) were estimated using published $(V-K)_0$ photometry. $T_{\rm eff}$ and microturbulence (V_t) were further refined via spectroscopic analyses. The analysis follows the methods described in Johnson et al. (2005) and Johnson & Pilachowski (2006).

4.1. *Model Stellar Atmospheres*

Using V photometry from van Leeuwen et al. (2000) and K_s photometry from 2MASS, we estimated $T_{\rm eff}$ with the color-temperature relation described in Alonso et al. (1999, 2001), which is based on the infrared flux method (Blackwell & Shallis 1977). However, the Alonso et al. (1999) method requires the photometry to be on the Carlos Sánchez Telescope (TCS) photometric system. We transformed the V and K_s magnitudes onto the TCS system using the transformations provided in Alonso et al. (1994, 1998) and Carpenter (2001), as summarized in Johnson et al. (2005). To correct for interstellar reddening and extinction, we applied the correction recommended by Harris (1996, rev. 2003 February) of $E(B-V) = 0.12$ and used $E(V-K)/E(B-V) = 2.7$ (Johnson 1965). While Calamida et al. (2005) claim differential reddening, perhaps differing by as much as a factor of 2 near the core, could be a problem, the well-defined evolutionary sequences seen in Villanova et al. (2007) seem to indicate it is not too severe. Van Loon et al. (2007) find some evidence for interstellar absorption by gas in the cluster, but this is concentrated near the core where our observations are sparse. Therefore, we have only applied a uniform reddening correction. Bolometric corrections were applied using the empirical relations given in Alonso et al. (1999) assuming a distance modulus of $(m-M)_V = 13.7$ (van de Ven et al. 2006).

Applying the proper color-temperature relation requires knowledge of a star's metallicity. Therefore, we took the empirical relation given in van Leeuwen et al. (2000; their eq. [15]), which gives [Ca/H] as a function of V and $B-V$, and assumed [Ca/Fe] ∼ +0.30 for [Fe/H] ≲ −1.0 (e.g., Norris & Da Costa 1995), with a linear decrease toward [Ca/Fe] = 0.0 at [Fe/H] = 0.0. This gave a rough estimate of [Fe/H] for each star and allowed us to choose the proper equation in Alonso et al. (1999).

Since only one Fe II line was available for analysis (6516 Å), we determined surface gravity using the standard relation,

$$\log(g) = 0.40(M_{\rm bol} - M_{\rm bol\odot}) + \log(g_\odot) + 4[\log(T/T_\odot)] + \log(M/M_\odot), \quad (1)$$

instead of the ionization equilibrium of Fe. We assumed $M = 0.80\ M_\odot$ for all stars, regardless of metallicity. Although there may be an intrinsic age spread of a few Gyr on the RGB (see § 5 for further discussion on this issue), this will lead to a mass difference only of order ∼0.05 $M_\odot$, which is negligible for surface gravity determinations.

In addition to $T_{\rm eff}$, $\log g$, and [Fe/H] estimates, we also needed a starting point with V_t. Initial estimates were based on the empirical relation derived in Pilachowski et al. (1996), which gives V_t as a function of $T_{\rm eff}$ for metal-poor field giants and subgiants. Typical V_t values ranged from about 1.3–2.3 km s^{-1} in the temperature range 5000–3800 K, respectively.

We generated the model stellar atmospheres by interpolating in the ATLAS9[5] (Castelli et al. 1997) grid of models without convective overshoot. Initial models were created using the $T_{\rm eff}$, $\log g$, [Fe/H], and V_t estimates as described above. $T_{\rm eff}$ was further refined by removing trends in Fe abundance as a function of excitation potential. Likewise, V_t was improved by removing trends in Fe abundance as a function of reduced width $[\log(\mathrm{EW}/\lambda)]$. A comparison between photometric and spectroscopically determined temperatures is given in the top panel of Figure 4. Typical photometric and spectroscopic temperature estimates agree to within approximately ±100 K. The bottom panel of Figure 4 shows our spectroscopically determined V_t as

[5] The model atmosphere grids can be downloaded from http://cfaku5.cfa.harvard.edu/grids.html.

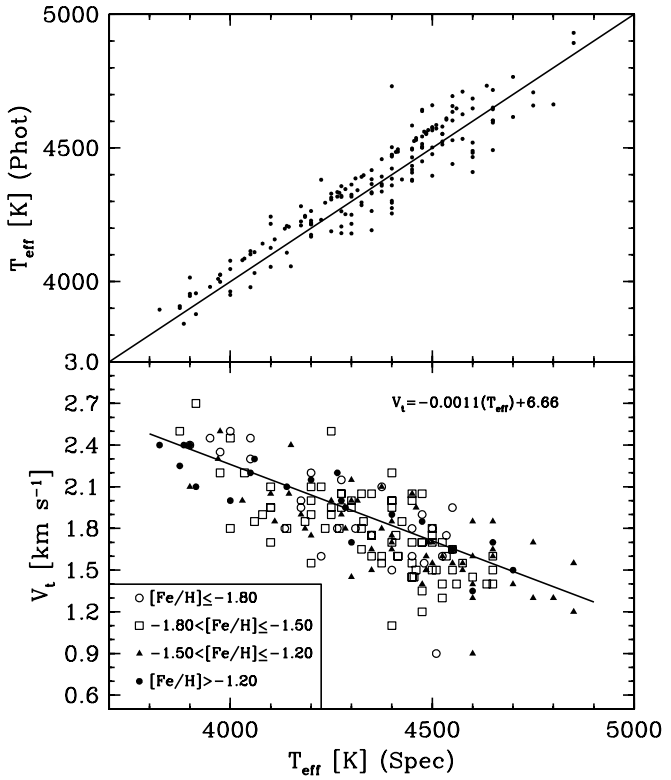

FIG. 4.— *Top*: Relation between the effective temperature estimated via $V - K$ photometry vs. the spectroscopically determined temperature. The straight line indicates perfect agreement. *Bottom*: Microturbulent velocity vs. effective temperature. Different symbols indicate stars in different metallicity bins as indicated above. A linear least-squares fit is provided along with the equation relating microturbulence to effective temperature.

a function of $T_{\rm eff}$ for different metallicity bins with a linear least-squares fit given by

$$V_t = -0.0011(T_{\rm eff}) + 6.66, \quad (2)$$

which is independent of metallicity. This fit agrees to within $\sim$0.10–0.15 km s^{-1} to that given in Pilachowski et al. (1996). Figure 5 shows our derived [Fe II/H] given as a function of [Fe/H]. As stated above, we only had one Fe II line available for analysis, but the fact that both Fe estimates agree to within 0.16 dex on average ($\sigma = 0.12$ dex) leads us to believe our surface gravity estimates are not in serious error. A complete list of our adopted model atmosphere parameters is provided in Table 3.

4.2. *Derivation of Abundances*

Abundances were determined using equivalent width analyses for all Fe lines and most Al lines, with the exception of cases where evidence for considerable CN contamination near the Al $\lambda\lambda$6696, 6698 doublet (i.e., metal-rich and/or CN-strong stars) existed and spectrum synthesis was used instead. We measured equivalent widths using a FORTRAN program developed for this project that interactively fits a Gaussian curve to each absorption line by implementing a Levenberg-Marquardt algorithm (Press et al. 1992) to find the least-squares fit given a continuum level and limits of integration. A high-resolution, high-S/N Arcturus spectrum[6] was simultaneously overplotted for each

[6] The Arcturus Atlas can be downloaded from the NOAO Digital Library at http://www.noao.edu/dpp/library.html.

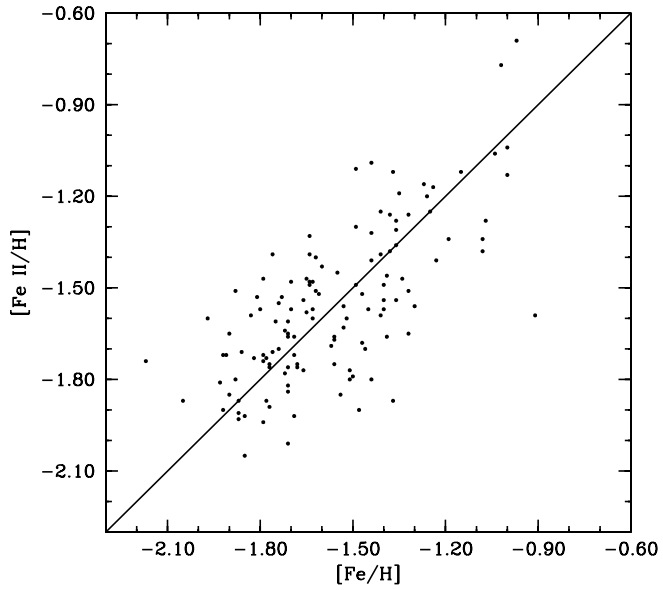

FIG. 5.—Derived [Fe II/H] abundances are plotted vs. [Fe I/H]. The line indicates perfect agreement.

spectrum to aide in continuum placement and line identification. The program also has the ability to fit up to five Gaussians simultaneously for deblending purposes; however, all equivalent widths were verified independently using IRAF's `splot` package.

4.2.1. *Equivalent Width Analysis*

Final abundances were calculated using the `abfind` driver in the 2002 version of the local thermodynamic equilibrium line analysis code MOOG (Sneden 1973). Adopted log gf values are the same as those employed in Johnson & Pilachowski (2006), which were adapted from line lists provided in Thévenin (1990), Sneden et al. (2004; modified from Ivans et al. 2001), and Cohen & Meléndez (2005). A summary of our line list is given in Table 4 and the measured equivalent widths are provided in Table 5.

While we had identified 20 Fe I lines for analysis, in most cases only 10–15 lines could be used due to severe line blending, bad CCD pixels, or line strength. In this sense, only lines lying on the linear part of the curve of growth were used, which meant neglecting almost all lines with a reduced width larger than about −4.5 (roughly 200 mÅ at 6600 Å). This unfortunately meant that many lines in metal-rich stars are too strong to give accurate abundances using our techniques. For the cases where Al abundances were determined using equivalent width measurements, weak line blends were taken into account using deblending methods. As stated above, stars with strong line blending or molecular line blanketing in the region near the Al doublet were analyzed with spectrum synthesis.

Typical uncertainties are quite small for [Fe/H] determinations with internal line-to-line spreads of $\sim$0.10–0.15 dex and $\sigma/\sqrt{N} < 0.05$ dex on average. Sample spectra for stars of approximately the same $T_{\rm eff}$ but different metallicities are shown in Figure 6. Here we illustrate that our [Fe/H] determinations are at the very least consistent in a relative sense as one notices the increasing Fe line strengths and CN-band strengths with increasing metallicity. The uncertainty in Al abundances is larger given that only two lines are available, but the two lines give a remarkably consistent abundance, with an average $\sigma/\sqrt{N} = 0.08$ dex. It should be noted that in several of our spectra only one Al line could be confidently measured due mostly to bad pixels. In Figure 6 the reader can see the stark contrast in line strength

TABLE 3
PHOTOMETRY AND MODEL ATMOSPHERE PARAMETERS

Star[a]	Alternate ID[b]	V	$B-V$	$V-K$ (TCS)	M_V^0	$T_{\rm eff}$ (K)	$\log g$ (cm s^{-2})	[Fe/H] Spectroscopy	V_t (km s^{-1})
9	370	12.529	1.250	2.870	−1.543	4460	1.20	−1.26	1.95
5009	548	12.912	1.080	2.841	−1.160	4525	1.40	−1.90	1.60
6017	240	12.233	1.420	3.387	−1.839	4110	0.85	−1.36	1.85
10012	43	11.529	1.618	3.782	−2.543	3900	0.40	−1.49	2.10
11019	537	12.841	1.223	2.985	−1.231	4450	1.30	−1.57	2.00
11024	91	11.738	1.333	3.291	−2.334	4200	0.70	−1.76	1.90
12013	394	12.579	1.319	3.142	−1.493	4275	1.10	−1.50	2.05
14010	435	12.807	0.993	2.647	−1.265	4635	1.45	−1.74	1.40
15022	180	11.982	1.243	2.997	−2.090	4400	0.95	−1.79	1.95
16009	252	12.232	1.201	3.081	−1.840	4375	1.00	−1.88	2.10

NOTE.—Table 3 is published in its entirety in the electronic edition of the *Astrophysical Journal*. A portion is shown here for guidance regarding its form and content.

[a] Identifier from van Leeuwen et al. (2000).

[b] Identifier from Woolley (1966).

between a star such as 51021, which has [Al/Fe] = +0.15 at [Fe/H] = −1.44, and star 61085, which has [Al/Fe] = +0.97 at [Fe/H] = −1.15. A summary of all derived abundances and associated $\sigma/\sqrt{N}$ values is given in Table 6.

4.2.2. *Spectrum Synthesis Analysis*

As mentioned above, we determined Al abundances for metal-rich and/or CN-strong stars using the synth driver in MOOG. Candidates for spectrum synthesis were chosen based on visual inspection of the 6680–6700 Å region, where the majority of lines surrounding the Al doublet are CN lines. Stars where CN contamination was seen between the Al lines were designated for synthetic spectrum analysis (e.g., see Fig. 6, *lower two spectra*).

TABLE 4
LINE LIST

Element	λ (Å)	Excitation Potential (eV)	$\log gf$
Fe II	6516.08	2.89	−3.45
Fe I	6533.93	4.56	−1.36
Fe I	6546.24	2.76	−1.54
Fe I	6551.68	0.99	−5.77
Fe I	6574.25	0.99	−5.02
Fe I	6592.92	2.73	−1.47
Fe I	6593.88	2.43	−2.42
Fe I	6597.57	4.79	−0.95
Fe I	6608.04	2.28	−3.96
Fe I	6609.12	2.56	−2.69
Fe I	6625.02	1.01	−5.37
Fe I	6627.54	4.55	−1.58
Fe I	6633.75	4.79	−0.80
Fe I	6646.96	2.61	−3.96
Fe I	6648.12	1.01	−5.92
Fe I	6677.99	2.69	−1.35
Al I	6696.03	3.14	−1.57
Al I	6698.66	3.14	−1.89
Fe I	6703.57	2.76	−3.01
Fe I	6710.32	1.48	−4.83
Fe I	6726.67	4.61	−1.07
Fe I	6733.15	4.64	−1.48
Fe I	6739.52	1.56	−4.79

NOTE.—Table 4 is also available in machine-readable form in the electronic edition of the *Astrophysical Journal.*

The atomic line list (with the exception of the two Al lines) was taken from the Kurucz atomic line database.[7] We adjusted the oscillator strengths from this line list so the line strengths matched those in the solar spectrum. For the CN molecular line list, we used a combination of one available from Kurucz and one provided by B. Plez (2007, private communication; for a description on how the line list was prepared, see Hill et al. 2002).

Since most of the program stars do not have known C, N, or $^{12}C/^{13}C$ abundances, we started with [C/Fe] = −0.5, [N/Fe] = +1.5, and $^{12}C/^{13}C = 5$, values roughly consistent with previous work (e.g., Norris & Da Costa 1995; Smith et al. 2002). We then treated the nitrogen abundance as a free parameter and adjusted it until a satisfactory fit was achieved. Typical best-fit [N/Fe] values were ∼+1.0 to +1.5. To test the effect of different $^{12}C/^{13}C$ ratios, we generated two sets of spectra with $^{12}C/^{13}C = 5$ and $^{12}C/^{13}C = 1000$. The fits to the CN lines were indistinguishable between the two cases, meaning ^{12}C is the dominant isotope in this spectral region and thus synthesized CN lines are insensitive to the ^{13}C abundance.

With the CN lines fit, we were then able to adjust the Al abundance until the synthetic spectrum matched the observed. Sample synthesis fits are given in Figure 7 for a metal-poor and metal-rich case. Aside from the CN lines, the Fe I line near the 6696 Å feature is the only other contaminating line in the region, but this line has an excitation potential of nearly 5 eV, making its contribution mostly negligible in these cool stars. Generally, the abundances given by the 6696 and 6698 Å lines agreed to within about ±0.10 dex. Since a significant percentage of our Al abundances were determined using synthesis analyses, we tested for systematic offsets between synthesis and equivalent width methods. For sample stars that were both metal-poor and did not show signs of CN contamination, the difference in [Al/Fe] determined via both methods was less than 0.05 dex. However, for higher metallicity stars and those with possible CN contamination, the difference was 0.10–0.20 dex, with equivalent width analyses always overestimating the abundance. The quoted values for Al abundances derived via spectrum synthesis are given as the average from those two lines. A summary of our derived abundances is given in Table 6. Stars with Al determinations via synthesis are designated by "Syn" in the 6696 and 6698 Å columns of Table 5.

[7] The Kurucz line list database can be accessed via http://kurucz.harvard.edu/linelists.html.

TABLE 5

EQUIVALENT WIDTHS

Star	λ^{a} = 6516	6533	6546	6551	6574	6592	6593	6597	6608	6609	6625	6627	6633	6646	6648	6677	6696	6698	6703	6710	6726	6733	6739
9[b]	63	20	151	...	...	159	130	34	40	100	51	14	...	15	36	170	...	23	...	...	28	...	49
5009	...	9	92	6	25	115	62	11	...	31	14	...	...	...	8	105	...	9	18	10	6	...	7
6017	41	30	140	...	108	179	134	25	52	102	105	16	...	39	82	202	Syn	Syn	91	81	31	25	49
10012	54	21	179	62	133	186	157	27	77	145	116	20	...	...	73	210	Syn	Syn	83	95	35	...	...
11019	...	13	139	18	68	141	118	17	17	82	24	8	...	...	15	141	22	18	...	22	24	...	33
11024	62	11	143	24	82	146	120	18	43	94	49	7	...	20	27	158	11	...	38	42	18	9	35
12013	...	18	149	31	89	165	145	22	37	...	74	17	...	...	...	161	Syn	Syn	61	64	...	9	...
14010	...	...	80	...	24	86	67	...	14	42	13	...	...	...	...	109	...	...	19	10	...	...	...
15022	48	5	119	...	53	121	101	...	19	...	26	...	...	12	...	142	13	...	...	19	16	...	14
16009	...	...	130	...	55	132	99	...	...	...	26	5	...	...	10	133	10	...	17	...	13	...	15

NOTE.—Equivalent widths are given in units of mÅ. The designation "Syn" indicates a synthetic spectrum comparison method was used. Table 5 is published in its entirety in the electronic edition of the *Astrophysical Journal*. A portion is shown here for guidance regarding its form and content.

[a] Wavelengths are given in units of Å.

[b] Designation is from van Leeuwen et al. (2000).

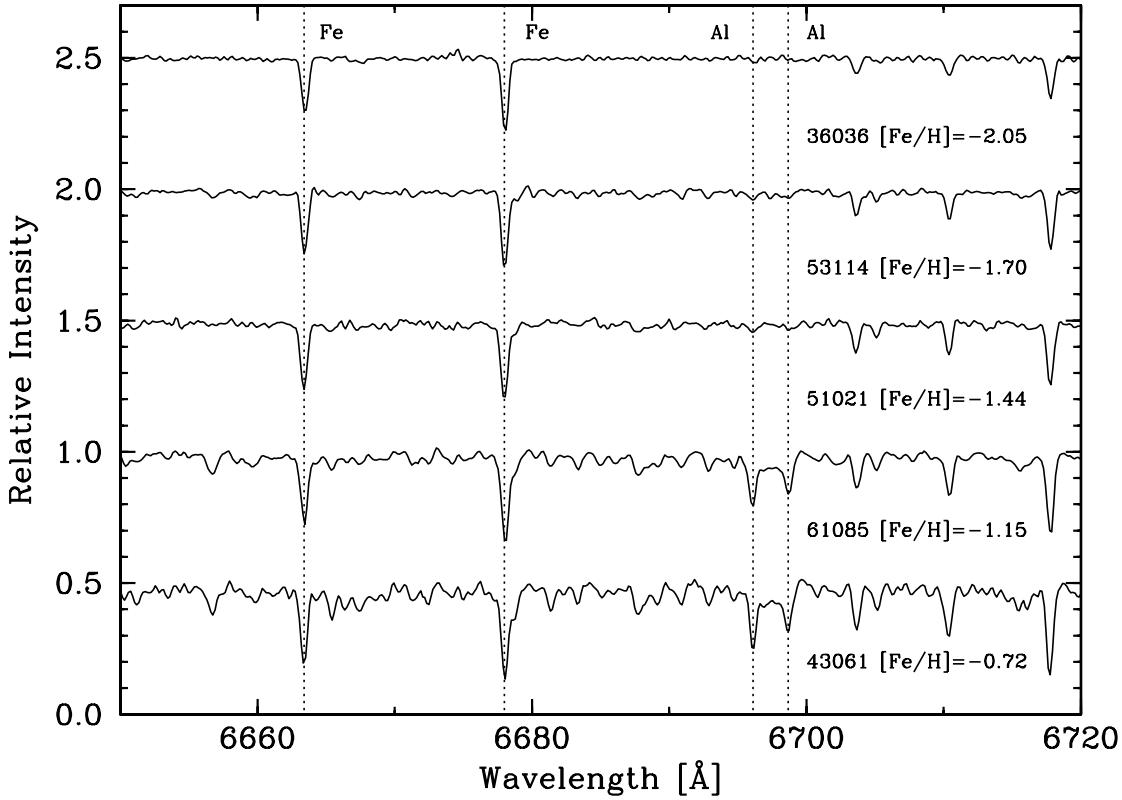

FIG. 6.— Several sample spectra are shown for various [Fe/H]. The spectra have been offset for display purposes. For reference the vertical dashed lines indicate the location of the Al I lines and two additional Fe I lines. From top to bottom, the [Al/Fe] values for the stars shown are +0.40, +0.45, +0.15, +0.97, and +0.57, respectively.

4.2.3. *Abundance Sensitivity to Model Atmosphere Parameters*

We tested the effects on derived abundances from changes in model atmosphere parameters by altering $T_{\rm eff} \pm 100$ K, $\log g \pm 0.25$ cm s^{-2}, and $V_t \pm 0.25$ km s^{-1} for models of [Fe/H] = −2.0, −1.5, and −1.0. As can be seen in Table 7, $T_{\rm eff}$ uncertainties are the primary source of error for Fe I and Al I, and surface gravity is the primary source for Fe II abundances. This seems logical given that Fe I and Al I reside in a subordinate ionization state, and Fe II exists in the primary ionization state.

Following Table 7, an uncertainty of order 100 K in $T_{\rm eff}$ leads to an error of ∼0.10–0.20 dex in Fe I, although the effect is somewhat reduced at higher metallicity. The opposite is true for Fe estimates based solely on the Fe II line, where the error range is ∼0.05–0.10 dex and the uncertainty becomes larger with increasing metallicity. Although the variation in Al I abundance as a function of $T_{\rm eff}$ uncertainty is smaller than for Fe I, it is still of order 0.10 dex with a weak dependence on metallicity.

The effects of surface gravity uncertainty are of order 0.10 dex for the Fe II line, but are negligible for the neutral Fe and Al lines. For this reason, enforcing ionization equilibrium between different species is often used for constraining surface gravity estimates. As mentioned in § 4.2.1, having only one Fe II line means the Fe abundance derived from Fe II is probably no more accurate than the typical line-to-line scatter present in Fe I ($\sigma \sim 0.10$–0.15 dex). Combined with the sensitivity of Fe II to surface gravity

TABLE 6
DERIVED ABUNDANCES

Star[a]	log ϵ(Fe)	[Fe/H][b]	Number of Lines	$\sigma/\sqrt{N}$	log ϵ(Al)	[Al/Fe][c]	Num. Lines	$\sigma/\sqrt{N}$
9	6.26	−1.26	14	0.03	5.78	0.57	1	...
5009	5.62	−1.90	15	0.05	5.39	0.82	1	...
6017	6.16	−1.36	18	0.05	6.28	1.17	2	0.07
10012	6.03	−1.49	16	0.03	5.35	0.37	2	0.02
11019	5.95	−1.57	16	0.03	5.53	0.63	2	0.11
11024	5.76	−1.76	19	0.03	4.94	0.23	1	...
12013	6.02	−1.50	14	0.03	5.13	0.16	2	0.07
14010	5.78	−1.74	10	0.03	...	...	...	...
15022	5.73	−1.79	12	0.04	5.14	0.46	1	...
16009	5.64	−1.88	11	0.03	5.04	0.45	1	...

NOTE.—Table 6 is published in its entirety in the electronic edition of the *Astrophysical Journal*. A portion is shown here for guidance regarding its form and content.

[a] Identifier from van Leeuwen et al. (2000).

[b] Assumed the solar log ϵ(Fe) = 7.52 (Sneden et al. 1991).

[c] Assumed the solar log ϵ(Al) = 6.47 (Anders & Grevesse 1989).

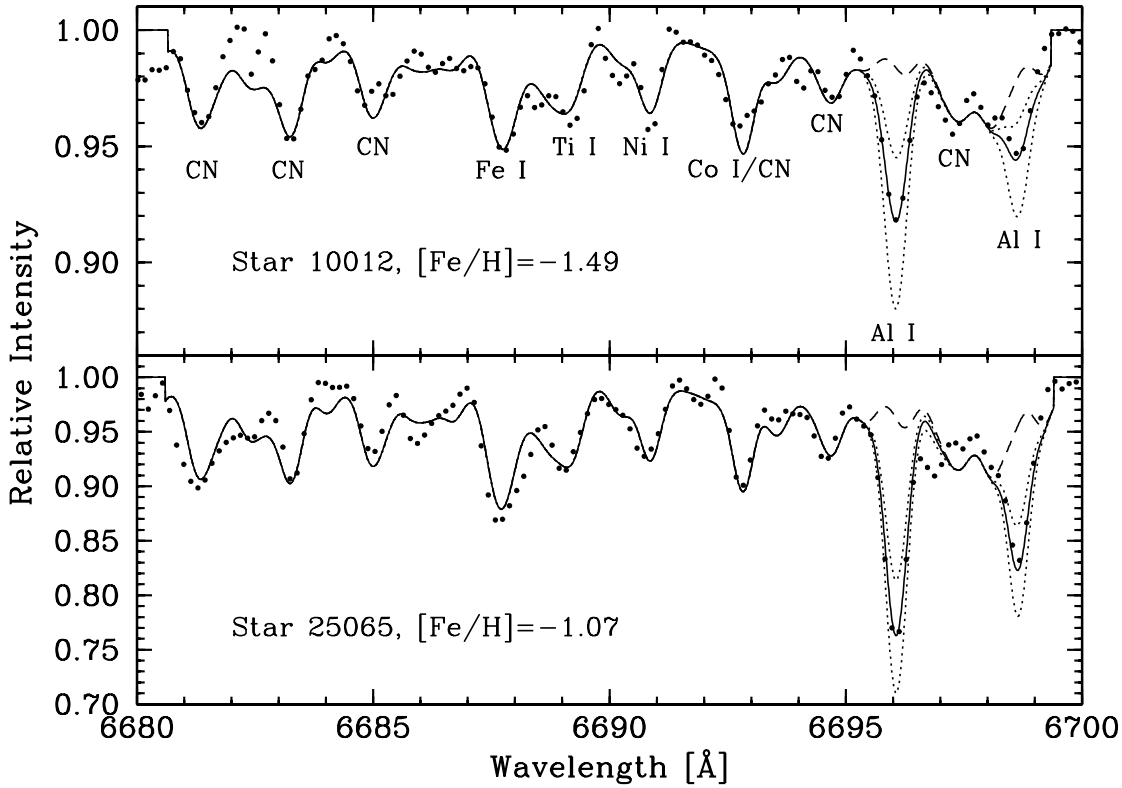

FIG. 7.—Sample spectrum syntheses of the Al region are shown. The dashed line indicates $\log \epsilon(\mathrm{Al}) = -5.0$, the solid line shows the best-fit Al abundance, and the dotted lines indicate abundance ±0.30 dex from the best-fit Al value.

estimates of order ±0.25 cm s^{-2}, the fact that agreement between Fe I and Fe II is better than about 0.10 dex (see Fig. 5) suggests estimates based on evolutionary arguments provide a decent approximation to the surface gravity; however, Table 7 shows this has little effect on our derived Fe I and Al I abundances. From this, we can safely assume that contamination from AGB stars, which have $M \sim 0.60\ M_{\odot}$ and thus a lower surface gravity, will not significantly alter our results.

The ad hoc microturbulence parameter, adjusted to remove abundance trends as a function of reduced width, has the strongest effect for lines lying on the flat part of the curve of growth. As is seen in Table 7, the effect on the Fe I abundance due to uncertainty in $T_{\rm eff}$ increases with increasing metallicity because the lines become progressively stronger. However, Fe II and Al I are mostly unaffected due to their relatively small equivalent widths and the effect on Fe I is still <0.10 dex even at $[\mathrm{Fe/H}] = -1.0$.

TABLE 7
ABUNDANCE SENSITIVITY TO MODEL PARAMETERS

Element	$\Delta T_{\rm eff} \pm 100$ (K)	$\Delta \log g \pm 0.25$ (cm s^{-2})	$\Delta V_t \pm 0.25$ (km s^{-1})	$\Delta N \pm 0.30$ (dex)
		$[\mathrm{Fe/H}] \approx -2.0$		
Fe I	±0.17	∓0.02	∓0.04	...
Fe II	∓0.05	±0.11	∓0.03	...
Al I	±0.07	∓0.02	±0.00	∓0.02
		$[\mathrm{Fe/H}] \approx -1.5$		
Fe I	±0.16	±0.00	∓0.06	...
Fe II	∓0.06	±0.12	∓0.04	...
Al I	±0.09	∓0.01	∓0.01	∓0.05
		$[\mathrm{Fe/H}] \approx -1.0$		
Fe I	±0.10	±0.01	∓0.08	...
Fe II	∓0.08	±0.11	∓0.04	...
Al I	±0.08	±0.00	∓0.01	∓0.08

In addition to variations in model stellar atmosphere parameters we tested the sensitivity of Al abundance to CN strength via spectrum synthesis by varying $[\mathrm{N/Fe}] \pm 0.30$ dex. Changing the nitrogen abundance by this amount worsens the fit to the CN lines in the spectrum, but alters the derived [Al/Fe] abundance less than 0.10 dex at all metallicities. Note that since [O/Fe] is unknown for most of our program stars and [O/Fe] can have values ranging from about +0.30 to less than −0.50, it is not possible to constrain the molecular equilibrium equations to derive true [C/Fe] and [N/Fe]. We present the [Al/Fe] results for each metallicity bin in Table 7.

4.3. *Comparison with the Literature*

While ω Cen has been the subject of multiple abundance studies (see § 1 for a brief review), most of these are low-resolution studies that do not involve elements other than Fe and/or Ca. Therefore, we are only comparing results in the literature for which moderate to high-resolution Al data are available and with which we have three or more stars in common. This limits the comparison to Brown & Wallerstein (1993; three stars), Norris & Da Costa (1995; 24 stars), Zucker et al. (1996; four stars), and Smith et al. (2000; three stars).

In Figure 8 we present the values of $T_{\rm eff}$, $\log g$, [Fe/H], and V_t given in the literature versus those obtained in this study. As can be seen from the figure, agreement is quite good for the temperature and surface gravity estimates, with the scatter increasing slightly for the metallicity and microturbulence estimates. For $T_{\rm eff}$, the average offset between our study and the literature is −7 K ($\sigma \sim 50$ K), and the average difference for $\log g$ is −0.02 cm s^{-2}

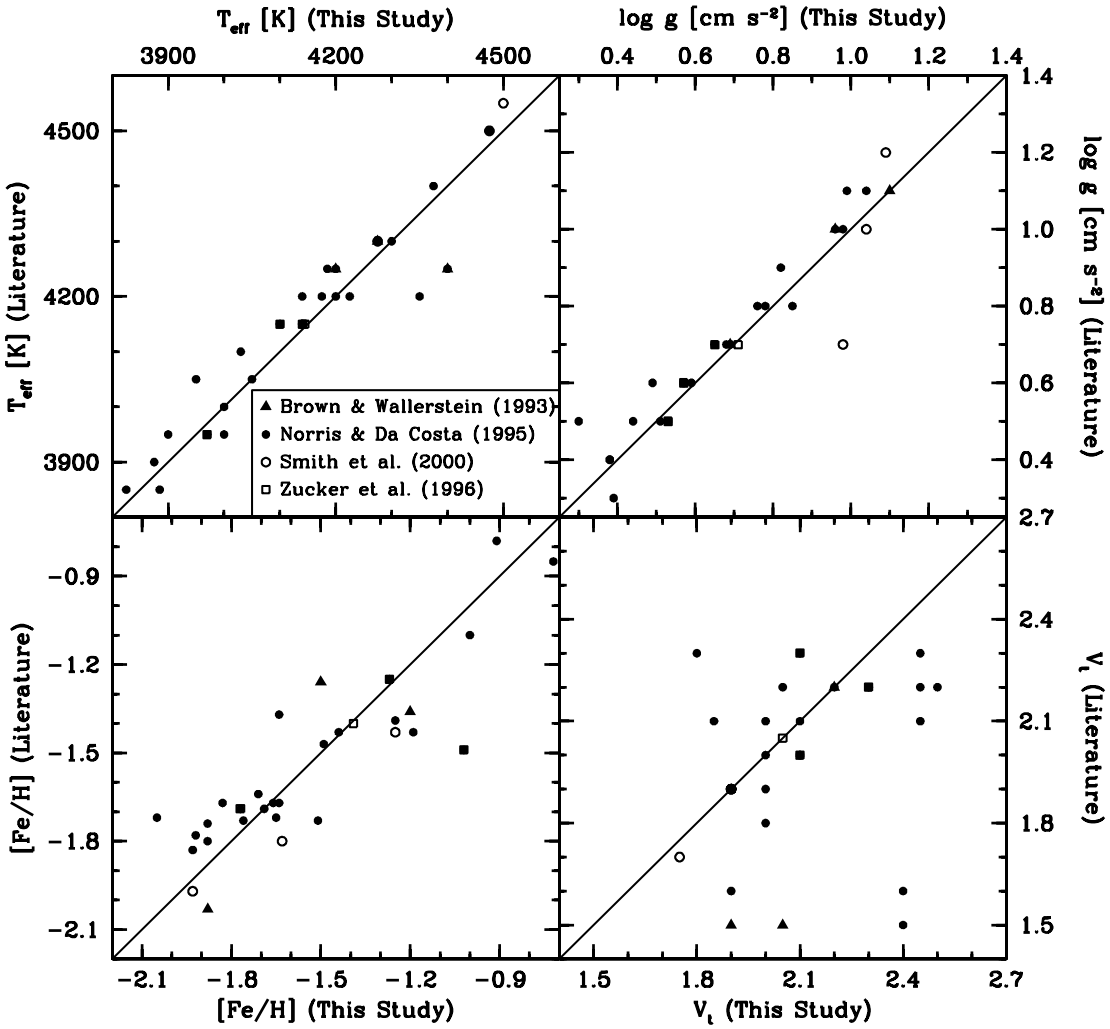

FIG. 8.—Four panels showing our adopted model atmosphere parameters vs. those available in the literature. A straight line indicates perfect agreement in all panels.

($\sigma \sim 0.10$ cm s^{-2}). This indicates that any disagreement between literature Fe and Al abundances and ours is not due to choices of $T_{\rm eff}$ and log g. Similarly, [Fe/H] measurements agree to within 0.02 dex on average ($\sigma \sim 0.20$ dex). The reason for the larger dispersion in microturbulence estimates is not entirely clear, but it could be due to factors such as the number of lines available, data quality, continuum placement, and type of lines used (i.e., high- and/or low-excitation potential). However, on average the agreement is within 0.10 km s^{-1} ($\sigma \sim 0.25$ km s^{-1}).

Comparison between our derived [Al/Fe] abundances versus those in the literature are provided in Figure 9. Given the various data qualities, choices of model atmospheres and parameters, and adopted atomic line data, agreement is again quite good. The average offset between our derived abundances and those available in the literature is 0.06 dex ($\sigma \sim 0.30$ dex). Given that typical uncertainties in [Al/Fe] are of order 0.10–0.20 dex, agreement is comparable to that range.

5. RESULTS AND DISCUSSION

5.1. Fe *Abundances*

As discussed in § 1, it has been known for many years and shown by several authors that ω Cen has a considerable spread in metallicity that ranges from slightly less than [Fe/H] = −2.0 to more than [Fe/H] = −0.7. While several lower resolution spectroscopic (Norris et al. 1996; Suntzeff & Kraft 1996; Sollima et al.

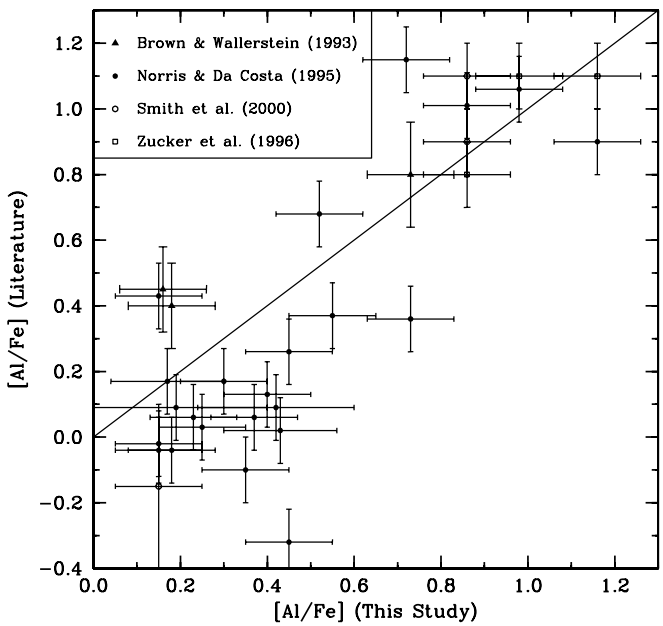

FIG. 9.—Al abundances available in the literature are plotted vs. those derived here. The straight line indicates perfect agreement. The error bars are those given from each study and this one. If no error is provided, a base value of ±0.10 dex is assumed.

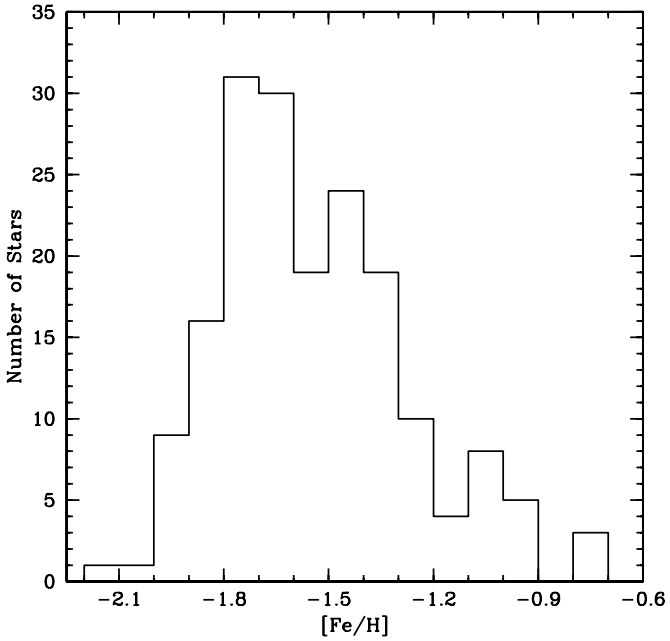

FIG. 10.—Histogram of derived [Fe/H] values with bin sizes of 0.10 dex.

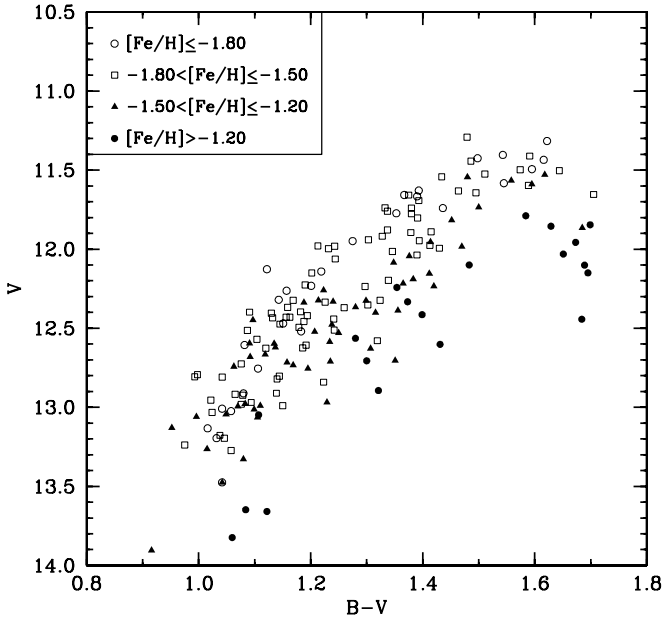

FIG. 11.—Color-magnitude diagram of program stars displayed in various metallicity bins as shown above.

2005b; Kayser et al. 2006; Stanford et al. 2006, 2007; van Loon et al. 2007[8]; Villanova et al. 2007) and photometric (Lee et al. 1999; Hilker & Richtler 2000; Hughes & Wallerstein 2000; Pancino et al. 2000; van Leeuwen et al. 2000; Rey et al. 2004; Stanford et al. 2004, 2006; Sollima et al. 2005a) studies have obtained metallicity estimates for a large number of stars ($N \gtrsim 500$ in some cases), there have only been a few high-resolution spectroscopic studies with a significant number ($N \gtrsim 10$) of stars observed (Norris & Da Costa 1995; Smith et al. 2000; Piotto et al. 2005; Sollima et al. 2006). However, aside from the present study, Norris & Da Costa (1995) still represents the largest ($N = 40$) single high-resolution analysis of ω Cen RGB stars. The general results from the metallicity studies can be summarized as: (1) few stars exist at $[\mathrm{Fe/H}] < -2.0$, (2) a primary peak in the metallicity distribution is observed at $[\mathrm{Fe/H}] \sim -1.8$ to -1.6, (3) there is a long tail of increasing metallicity up to $[\mathrm{Fe/H}] \sim -0.5$, and (4) there appear to be multiple peaks in the distribution at various [Fe/H] values.

In Figure 10 we present a histogram of our derived metallicity distribution function for all 180 stars. We find in agreement with previous studies that there are at least four distinct populations with the most metal-poor having $[\mathrm{Fe/H}] \sim -1.75$, the two intermediate-metallicity populations have $[\mathrm{Fe/H}] \sim -1.45$ and -1.05, and the most metal-rich population has $[\mathrm{Fe/H}] \sim -0.75$. While our observations are skewed toward observing more metal-poor stars (see Fig. 2), there are intrinsically more metal-poor than metal-rich stars, as can be seen in Figure 1. This means our derived metallicity distribution is affected by *both* the actual distribution *and* observational selection effects. Given that we only observed one star on the most metal-rich branch, it is possible that stars with metallicities higher than $[\mathrm{Fe/H}] = -0.75$ exist. However, since our observed completion fraction is significantly higher for the most metal-poor stars, it is likely that our observed distribution function is accurate in a relative sense such that the cluster was rapidly enriched from the primordial metallicity of $[\mathrm{Fe/H}] \sim -2.15$ to the first major epoch of star formation at $[\mathrm{Fe/H}] \sim -1.75$. The absence of stars more metal-poor than $[\mathrm{Fe/H}] \sim -2.2$ means the proto-ω Cen environment was already preenriched, perhaps from processes such as cloud-cloud collisions (Tsujimoto & Shigeyama 2003), when the primary metal-poor population formed. In contrast, field stars in the Galactic halo exhibit a wide range of metallicities from $[\mathrm{Fe/H}] > 0.0$ to $[\mathrm{Fe/H}] < -4.0$ (e.g., Gratton et al. 2004), indicating that the two do not share a common chemical enrichment history.

The distribution shown in Figure 10 suggests that if ω Cen evolved as a single entity (i.e., without significant contributions from mergers), then there were four to five significant star formation episodes that occurred. This seems to fit the high-resolution photometric data from Sollima et al. (2005a) and Villanova et al. (2007) that show the multiple giant branches appear in discrete groups instead of as a continuous distribution. This trend is similarly reproduced in Figure 11, where our derived metallicities are superimposed on the photometric data from van Leeuwen et al. (2000). Here, even when binning by the approximate 3 σ value of each peak in the distribution from Figure 10 (0.3 dex), the different metallicity groups can be separated. The metallicity distribution from Figure 10 is very well produced in the hydrodynamical chemical enrichment simulations of Marcolini et al. (2007), where they assumed ω Cen is the core remnant of a dwarf spheroidal galaxy that was captured and tidally stripped ~10 Gyr ago with star formation occurring over roughly 1.5 Gyr. The simulated metallicity peaks from Marcolini et al. (2007) lie at $[\mathrm{Fe/H}] \sim -1.6, -1.35, -1.0$, and -0.70, which are very similar to ours at $[\mathrm{Fe/H}] = -1.75, -1.45, -1.05$, and -0.75.

There is some evidence that different metallicity populations may be spatially and kinematically unique (Norris et al. 1996; 1997; Suntzeff & Kraft 1996; Hilker & Richtler 2000; Pancino et al. 2000; 2003). In Figure 12 we present Fe and Al abundances as a function of distance from the cluster center. Keeping in mind our observational bias, we find a marginal tendency for the more metal-rich stars to be located in the inner regions of the cluster while the more metal-poor stars are rather evenly distributed at all radii sampled here. However, given our small

[8] The referee noted discrepancies between the [Fe/H] values derived by Norris & Da Costa (1995) and van Loon et al. (2007). We note that our results agree with Norris & Da Costa and a detailed resolution of this problem is beyond the scope of this paper.

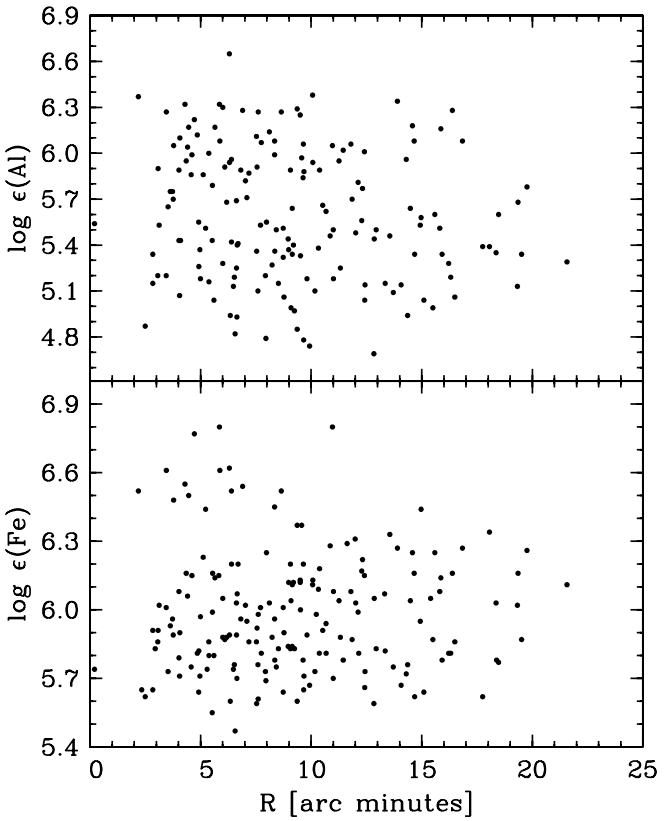

FIG. 12.— Al and Fe are plotted as a function of radial distance from the cluster center.

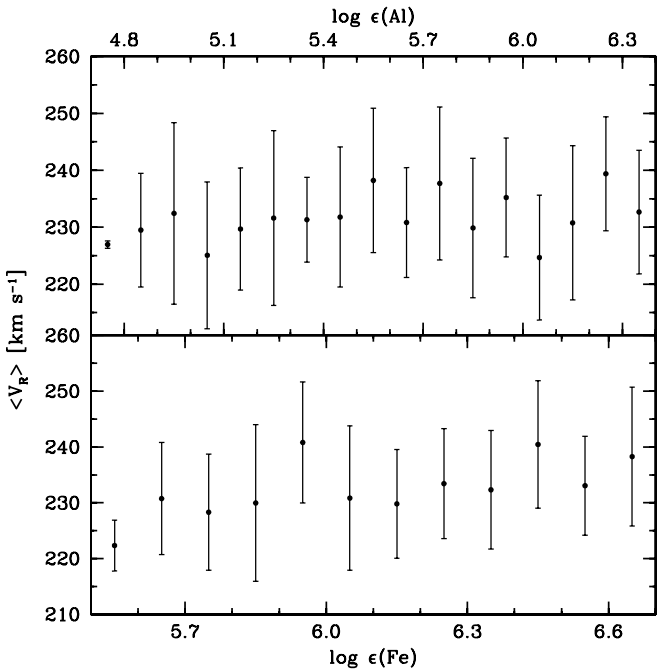

FIG. 13.— *Top*: Average radial velocity vs. log ϵ(Al) and the bottom panel is for log ϵ(Fe). The filled circles represent average radial velocities in each abundance bin and the vertical bars indicate the velocity dispersion in each bin. Both panels have a bin size of 0.10 dex in abundance.

sample size in the metal-rich regime, we are unable to make any definitive arguments for or against a metallicity-radius relationship. It should be noted although that Ikuta & Arimoto (2000) and Rey et al. (2004) do not find any strong evidence for the metal-poor and metal-rich populations having a spatially different structure. Even though the relaxation time for ω Cen is thought to exceed 5 Gyr (Djorgovski 1993; Merritt et al. 1997), any correlation between projected spatial position and metallicity is apparently subtle. However, it has been pointed out in deep photometric surveys (e.g., Rey et al. 2004) that the most metal-rich RGB-a is predominately seen in CMDs of the inner region of the cluster.

The main result indicating that at least the most metal-rich population may have a different formation history is that those stars appear to have a lower velocity dispersion (i.e., are kinematically cooler) than the other populations and do not show signs of rotation (Norris et al. 1997). In Figure 13 we show our derived radial velocities plotted both as a function of log ϵ(Fe)[9] and log ϵ(Al), where the error bars indicate the velocity dispersion in the data. To within one standard deviation, we do not find significant evidence for any of the stellar populations having a different bulk radial velocity or velocity dispersion. It seems unlikely that a larger sample size would provide significantly different results because Reijns et al. (2006) determined radial velocities for nearly 2000 ω Cen members and concluded the RGB-a stars had radial velocity and dispersion values consistent with the entire cluster. Pancino et al. (2007) have shown the rotational velocities for all populations are comparable to one another, but interestingly they find an underlying sinusoidal pattern in their measured velocities as a function of position angle. However, the metal-poor, intermediate-metallicity, and anomalous giant branches all show the same sinusoidal pattern. Whether any true kinematic anomaly exists for this cluster or not remains to be seen.

[9] That is, $\log \epsilon(\mathrm{X}) = \log (N_{\mathrm{X}}/N_{\mathrm{H}}) + 12$.

5.2. Al *Abundances*

The bulk of aluminum production in galaxies and globular clusters is thought to arise from quiescent carbon and neon burning in massive stars ($M \gtrsim 8\,M_{\odot}$) and HBB occurring in the envelopes of IM-AGB stars via the MgAl cycle (e.g., Arnett & Truran 1969; Arnett 1971). In most Galactic globular clusters, there is a very small (<0.10 dex) spread in the abundance of heavy α and Fe-peak elements, with a somewhat larger spread ($\sim$0.3–0.6 dex) in *s*- and *r*-process elements (e.g., Sneden et al. 2000). However, the lighter elements carbon through aluminum are typically not uniform and in some cases show star-to-star variations of more than a factor of 10. While ω Cen does not share all of the same chemical characteristics as globular clusters, the primary production locations of each element should be similar to globular clusters and/or the Galactic halo. The lesson learned from the monometallicity of "normal" globular clusters is that however Al manifests itself onto the surface of stars, the process must not alter Fe-peak, *s*-process, or *r*-process abundance ratios. This means that the often large star-to-star variation of [Al/Fe] seen in globular clusters (but not in halo field stars) are not due to supernova yields or the *s*-process, leaving either in situ deep mixing or HBB as the possible sites for [Al/Fe] variation. With these two scenarios in mind, we explore Al abundances with the goal of helping to constrain the source of Al variation and chemical evolution in ω Cen.

While the literature on Fe abundances for both evolved and main-sequence stars is quite extensive, the spectroscopic surveys by Norris & Da Costa (1995) and Smith et al. (2000) represent the only studies to consider light-element abundances that include Al for a large ($N \geq 10$) number of RGB stars in ω Cen. The results of those two studies indicate that the full range of

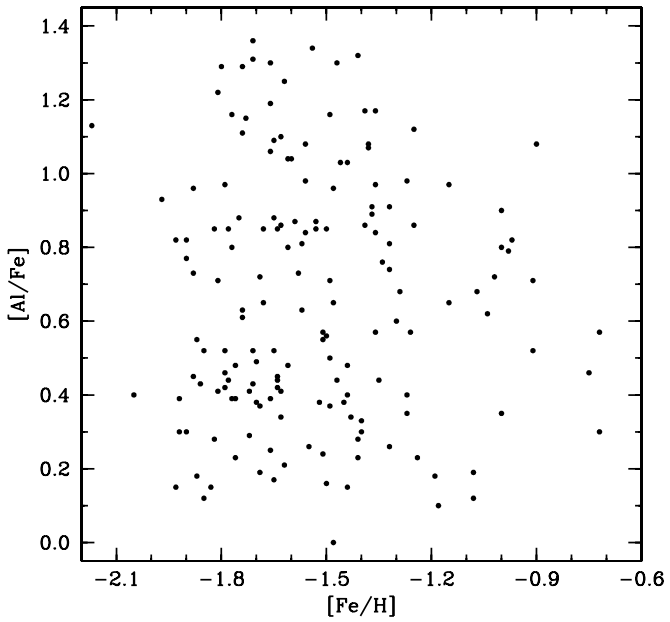

FIG. 14.—[Al/Fe] plotted as a function of [Fe/H].

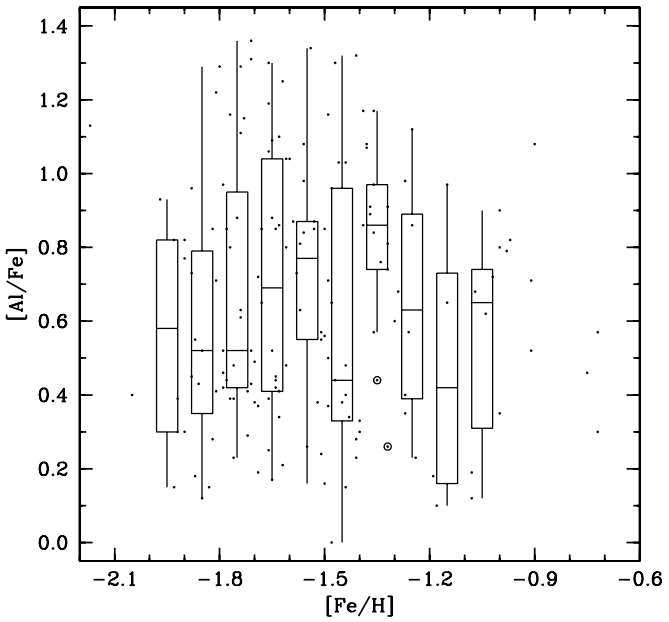

FIG. 15.—Box plot is shown on top of the [Al/Fe] vs. [Fe/H] plot given in Fig. 14. The data are binned into 0.10 dex intervals with the boxes centered on each bin. The middle line of each box indicates the median value, the lower and upper bounds of the box are the first and third quartile, the vertical lines are the full data range neglecting outliers, and the open circles indicate data lying 1.5–3.0 times the interquartile range away from either boundary.

[Al/Fe] is larger than 1.0 dex, Al and Na are correlated, Al and O are anticorrelated, and there is a hint of a decrease in [Al/Fe] with increasing [Fe/H]. We present the results of our larger sample plotting [Al/Fe] as a function of [Fe/H] in Figure 14. Even for the lowest metallicity stars, a large range in [Al/Fe] of $\sim$0.70 dex is already present. Near the first metallicity peak at $[\mathrm{Fe/H}] = -1.75$, where it is assumed the first episode of star formation after the initial enrichment period occurred, the full range in [Al/Fe] reaches a maximum value of $\sim$1.3 dex. This star-to-star variation remains mostly constant until about $[\mathrm{Fe/H}] = -1.4$, where the variation begins to decrease smoothly with increasing [Fe/H]. Interestingly, the "floor" Al abundance remains mostly constant at $[\mathrm{Al/Fe}] \sim +0.15$, regardless of the star's metallicity; a characteristic shared with many globular clusters of various metallicity and in agreement with [Al/Fe] values typical of Galactic halo stars in ω Cen's metallicity regime.

In Figure 15 we overlay a box plot on top of the underlying distribution from Figure 14. The median [Al/Fe] ratio typically resides between about 0.45 and 0.80 dex for all well-sampled metallicities, with a relatively constant interquartile range. This implies that the average amount of Al in the cluster must increase with increasing Fe abundance, at least up to $[\mathrm{Fe/H}] \sim -1.4$. This result is confirmed in Figure 16, where $\log \epsilon(\mathrm{Al})$ is plotted against $\log \epsilon(\mathrm{Fe})$. It appears that for metallicities higher than about $\log \epsilon(\mathrm{Fe}) = 6.0 ([\mathrm{Fe/H}] \approx -1.50)$, $\log \epsilon(\mathrm{Al})$ no longer increases beyond $\log \epsilon(\mathrm{Al}) \approx 6.40$ and the star-to-star scatter decreases. This result is likely robust against our observational bias because all stars observed in the metal-rich regime are located at or near the RGB tip (see Fig. 1), where it is believed any Al enhancements due to deep mixing should be the most apparent. However, no obvious trend is seen between Al abundance and evolutionary state.

As discussed previously, there is some evidence for a correlation between Fe abundance and distance from the cluster center and we show the results from this study in the bottom panel of Figure 12. In the top panel of Figure 12, we present the same data but for Al instead of Fe. While there may be a tendency for the most metal-rich stars to be located inward of about 10′–15′, there is no evidence of a trend for Al. Instead, stars of varying Al abundance are uniformly spread throughout the entire region sampled, at least out to $\sim$20′. Likewise, the top panel of Figure 13 shows average radial velocities for Al abundances in 0.10 dex bins. To within uncertainties, there appears to be no trend in either radial velocity or velocity dispersion with $\log \epsilon(\mathrm{Al})$. The fact that we do not find any preference of Al abundance or star-to-star dispersion with distance from the cluster center or radial velocity suggests star formation occurred on timescales shorter than those required to uniformly mix the gas.

5.3. *Possible Implications on Chemical Evolution*

From our available spectroscopic data for 180 RGB stars, we have confirmed the existence of at least four stellar populations

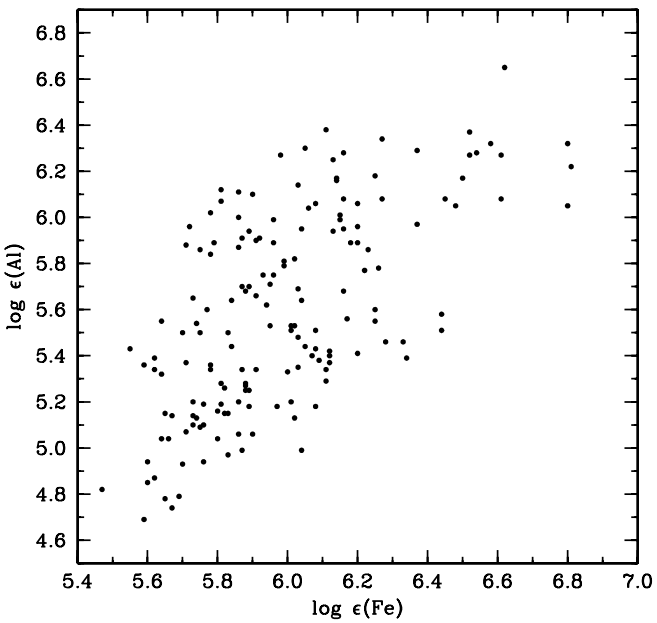

FIG. 16.—Plot of $\log \epsilon(\mathrm{Al})$ as a function of $\log \epsilon(\mathrm{Fe})$.

ranging in metallicity in the range $-2.2 < [\mathrm{Fe/H}] < -0.70$, in agreement with previous photometric, low-resolution spectroscopic, and smaller sample high-resolution spectroscopic studies. In addition, we have determined [Al/Fe] abundances for about 165 giants, most of which for the first time, with a sample larger by more than a factor of 4 than what was previously available in the literature. We find a constant Al abundance floor of $[\mathrm{Al/Fe}] \sim +0.15$ present at all metallicities, but with a largely varying and metallicity dependent spread above the floor. The star-to-star variation reaches a maximum extent in the intermediate-metallicity regime, which is consistent with the second peak in the metallicity distribution, and begins to decline at higher metallicities. The floor itself is consistent with observations of field stars and is predicted by Galactic chemical evolution models, but the large [Al/Fe] variations are not predicted. Observations of some Galactic globular cluster stars, especially more metal-poor than $[\mathrm{Fe/H}] \sim -1.5$, show similar large star-to-star variations in [Al/Fe]. Combining our determined Fe and Al abundances with those available in the literature for these and other elements now allows us to examine each metallicity regime in turn.

5.3.1. *The Metal-Poor Population*

A prominent feature of the metal-poor stars ($[\mathrm{Fe/H}] \lesssim -1.6$) in ω Cen is the rapidly increasing abundances of Na, Al, and light and heavy *s*-process elements relative to Fe as the metallicity increases from $[\mathrm{Fe/H}] = -2.2$ to the first metallicity peak at $[\mathrm{Fe/H}] = -1.75$ (e.g., Norris & Da Costa 1995; Smith et al. 2000). These increases are accompanied by nearly constant heavy $[\alpha/\mathrm{Fe}] \sim +0.30$, low Cu abundances ($[\mathrm{Cu/Fe}] \sim -0.60$), and low *r*-process abundances ($[\mathrm{Eu/Fe}] \sim -0.50$). These results seem to indicate that massive stars exploding as Type II SNe are the primary contributors for Fe-peak and heavy α-element enhancement in the cluster, but the low Eu abundances, which should be synthesized in the same stars, are puzzling. In addition, the growing *s*-process component appears to be best fit by models of 1.5–3 $M_{\odot}$ AGB ejecta (Smith et al. 2000). The lack of clear evidence for Type Ia SNe having contributed to the chemical composition of metal-poor stars in ω Cen (e.g., Smith et al. 2000; Cunha et al. 2002; Pancino et al. 2002; Platais et al. 2003) is consistent with the $\gtrsim$1 Gyr timescales needed for Type Ia SNe to evolve and the fact that they might not efficiently form in metal-poor environments (Kobayashi et al. 1998).

As mentioned above, the majority of Al present in the atmospheres of these RGB stars was likely produced in Type II SNe explosions that polluted the pristine gas from which these stars formed. While the heavy element data do not support high-mass ($\gtrsim 8\,M_{\odot}$) stars being the source for the more than 1.0 dex [Al/Fe] variations, that may be explained from HBB occurring in IM-AGB stars, in situ deep mixing, or a hybrid scenario. In Figures 14–16 we have shown that $[\mathrm{Al/Fe}] \geq 0$ for *all* metal-poor stars sampled, but a constant Al abundance floor is setup at $[\mathrm{Al/Fe}] \sim +0.15$ with a rapidly increasing star-to-star dispersion that reaches about 1.3 dex in extent by $[\mathrm{Fe/H}] = -1.75$. For the neutron capture elements, which are the only other group exhibiting a variations with metallicity, Smith et al. (2000) showed stars with $[\mathrm{Fe/H}] \sim -2$ are dominated by an *r*-process component with a shift to a primarily *s*-process component by $[\mathrm{Fe/H}] \gtrsim -1.8$.

In the pure pollution scenario, which does not invoke deep mixing affecting elements heavier than N, Type II SNe, low and IM-AGB stars, and perhaps winds from less evolved very massive stars (e.g., Maeder & Meynet 2006) are responsible for all abundance anomalies. Adding our large Al data set to the sample of stars previously observed may help constrain enrichment timescales and polluting AGB masses. Conventional theory suggests light and *s*-process elements do not share the same origin and ω Cen's *s*-process component is best fit with lower mass AGB stars, but masses lower than $\sim$3–4 $M_{\odot}$ undergo third dredge-up without significant HBB (e.g., Karakas & Lattanzio 2007) and thus should not appreciably alter their envelope Al abundances. In addition, Ventura & D'Antona (2008a) suggest globular cluster light-element anomalies can only be explained with ejecta from AGB stars in the mass range of $\sim$5–6.5 $M_{\odot}$. While our sample only includes two stars with $[\mathrm{Fe/H}] < -2$ (36036 and 51091), the elevated [Al/Fe] ratios of +0.40 and +1.13 suggest IM-AGB stars, with lifetimes of about $(50\text{–}150) \times 10^6$ yr (Schaller et al. 1992), have already polluted the ω Cen system. In this case, the low-metallicity environment would favor high [Al/Fe] yields from HBB processes occurring in IM-AGB stars. The rapidly rising average value of $\log \epsilon(\mathrm{Al})$ shown in Figure 16 in the metallicity regime $-2.0 \lesssim [\mathrm{Fe/H}] \lesssim -1.6$ implies a continued contribution from IM-AGB stars, presumably forming from the same star formation event that creates the first peak in the metallicity distribution. The top two panels of Figure 17 show binned [Al/Fe] for this metallicity regime, and we note approximately four subpopulations with $[\mathrm{Al/Fe}] \sim +0.15, +0.45, +0.85$, and $>+1.05$. Predicted yields from Type II SNe (e.g., Woosley & Weaver 1995) and measurements of field stars (e.g., Fulbright 2002) suggest Type II SNe should enrich the ISM with $[\mathrm{Al/Fe}] \sim +0.10$ to +0.30 while $\sim$5–6.5 $M_{\odot}$ AGB stars should produce $[\mathrm{Al/Fe}] \sim +0.50$ to +1.10 (e.g., D'Antona & Ventura 2007), which could explain our observed distribution. Given the rather short lifetimes of stars believed to produce Al and the fact that evidence for 1.5–3.0 $M_{\odot}$ pollution does not appear until $[\mathrm{Fe/H}] \sim -1.8$, it would seem that ω Cen was probably enriched from $[\mathrm{Fe/H}] = -2.2$ to -1.75 in $\sim$0.5–1.0 Gyr.

5.3.2. *The Intermediate-Metallicity Populations*

For the two intermediate-metallicity populations ($[\mathrm{Fe/H}] = -1.45$ and $[\mathrm{Fe/H}] = -1.05$), the heavy $[\alpha/\mathrm{Fe}]$ ratio remains constant and the *s*-process abundances level off with very little star-to-star dispersion (Norris & Da Costa 1995; Smith et al. 2000). As in the most metal-poor stars, *r*-process and Cu ratios relative to Fe remain low and mostly unchanged. However, the star-to-star scatter in O, Na, and Al is still quite large. It is interesting to point out that $\log \epsilon(\mathrm{Al})$ reaches its maximum value at about the same metallicity at which the *s*-process elements reach a constant ratio relative to Fe. The [Al/Fe] abundance floor is constant throughout this metallicity regime at $[\mathrm{Al/Fe}] \sim +0.15$, which means the scatter, still considerably larger than for [Ba/Fe], decreases as a function of increasing metallicity. This trend should presumably be present for Na and in the opposite sense for O assuming the Na-Al correlation and O-Al anticorrelation exist at all metallicities.

Had the scatter in Al abundances been comparable to that of other heavier elements in this metallicity range ($\sim$0.10–0.30 dex) with a nearly constant [Al/Fe] ratio, as is seen in field stars, we might be inclined to believe Al enhancement in the cluster was due solely to production in massive stars and that typical Type II SNe ejecta have $[\mathrm{Al/Fe}] \sim +0.15$. It is interesting to note that the [Al/Fe] floor tracks closely (with a slight offset of $\sim$0.2–0.3 dex) to the Galactic chemical evolution model presented in Timmes et al. (1995; their Fig. 19), assuming the amount of Fe ejected is decreased by a factor of 2, and Samland (1998; their Fig. 10), with an increase in secondary (i.e., metal-dependent) Al production by a factor of 5. If the well-known light-element correlations/anticorrelations seen in previously observed ω Cen stars (e.g., Norris & Da Costa 1995) holds at all metallicities and for all stars, those with $[\mathrm{Al/Fe}] \sim +0.15$ should also have $[\mathrm{O/Fe}] \sim +0.30$,

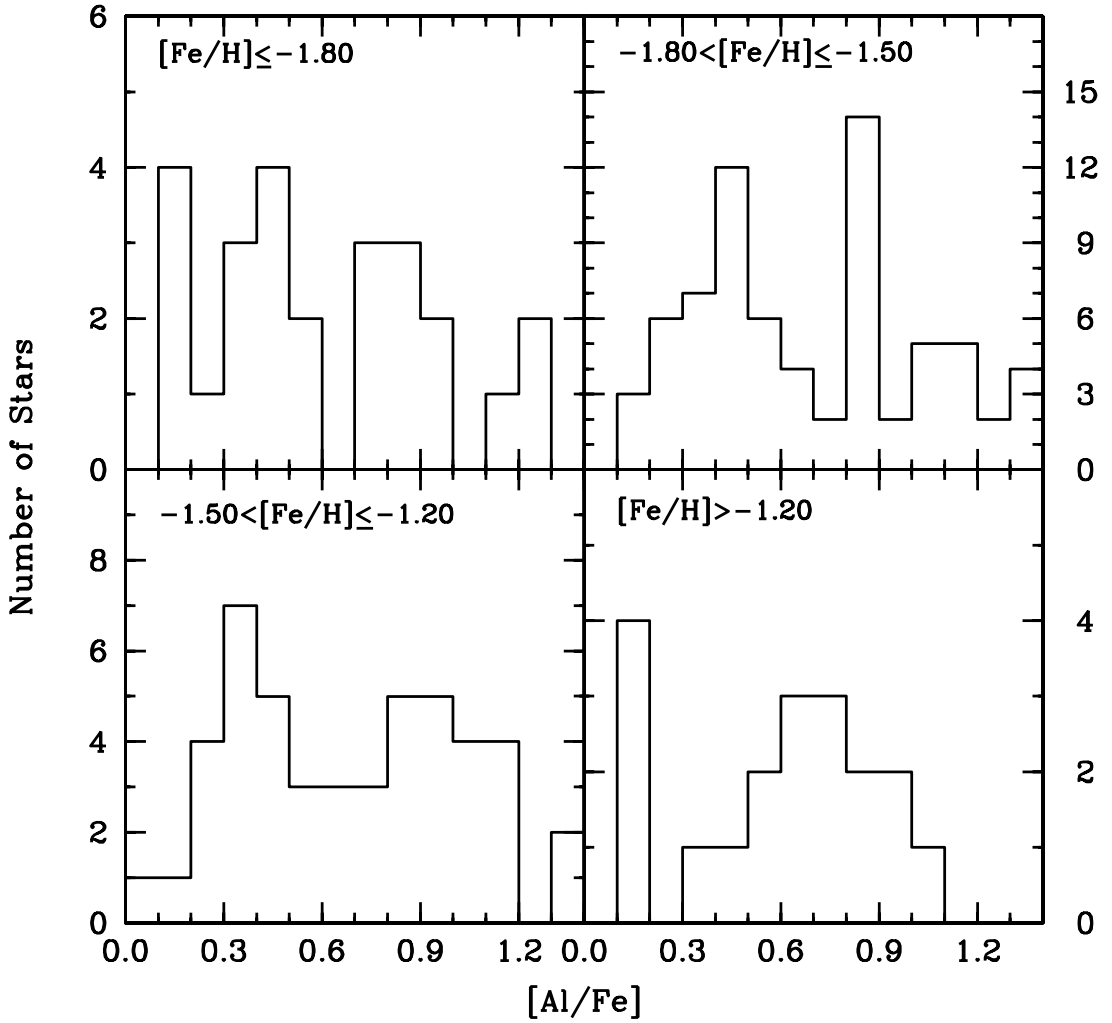

FIG. 17.—Histograms of [Al/Fe] using a bin size of 0.10 dex for multiple metallicity bins.

heavy $[\alpha/\mathrm{Fe}] \sim +0.30$, and $[\mathrm{Na/Fe}] \sim -0.20$, which are consistent with predicted yields from Type II SNe (e.g., Woosley & Weaver 1995). It could be that these stars formed preferentially out of SNe ejecta without significant IM-AGB contamination.

While the maximum observed $\log \epsilon(\mathrm{Al})$ increases with metallicity for the most metal-poor ω Cen giants, this trend halts at $[\mathrm{Fe/H}] \sim -1.4$, which coincides with the second peak in the metallicity distribution (i.e., the next round of star formation). We know the heavy $[\alpha/\mathrm{Fe}]$, [Ba/Fe], and floor [Al/Fe] ratios remain constant at higher metallicities, indicating an increase in $\log \epsilon(\mathrm{Ba})$, $\log \epsilon(\alpha)$, and the minimum $\log \epsilon(\mathrm{Al})$ that track with Fe. The question now posed by the Al data is why does the process producing the high Al values shut off or become less efficient at $[\mathrm{Fe/H}] \gtrsim -1.45$? Increases in metallicity lead to lower temperatures at the bottom of the convective envelope and require higher masses for HBB to occur. It may be that we are observing the result of lower convective efficiency at higher metallicity and/or that fewer IM stars form in higher metallicity environment. IM-AGB models in the metallicity range of $-1.5 \lesssim [\mathrm{Fe/H}] \lesssim -0.7$ (e.g., Fenner et al. 2004; Ventura & D'Antona 2008a, 2008b) predict [Al/Fe] yields of $\sim$+0.5 to +1.0, with lower [Al/Fe] yields at higher [Fe/H]. This may explain the bimodal distribution in the bottom panels of Figure 17, with the abundances in between possibly being due to varying degrees of ejecta dilution. The fact that the metallicity at which the heavy elements cease to increase in abundance more quickly than Fe and the metallicity where the maximum [Al/Fe] begins to decrease coincide suggests an important parameter changed in ω Cen at this point in its evolution. It may even be the case that this is when the progenitor dwarf galaxy began to change structurally via encounters with the Galactic disk. It appears that at metallicities higher than $[\mathrm{Fe/H}] = -1.45$, the cluster slowly approaches a constant [Al/Fe], which is consistent with values observed in the halo.

While Type Ia ejecta have been mostly ruled out by previous studies as contributors to the most metal-poor population, the metallicity at which they become important contributors is unclear. Marcolini et al. (2007) claim that their intermediate-metallicity peak at $[\mathrm{Fe/H}] \sim -1.4$ is due primarily to inhomogeneous pollution by Type Ia SNe. It is interesting to note that in this same metallicity bin we find a median [Al/Fe] value about 0.40 dex lower than the two surrounding bins, as well as the only star with $[\mathrm{Al/Fe}] \lesssim +0.15$. It is uncertain whether this is a real effect or simply due to an anomalous selection of stars. Inhomogeneous pollution by Type Ia SNe may also explain the bimodal distribution seen in the bottom panels of Figure 17 where stars polluted by both Type Ia ejecta and IM-AGB stars exhibit lower [Al/Fe] ratios and "normal" stars polluted by Type II SNe and IM-AGB stars have higher [Al/Fe] values. While the same trend is not particularly apparent for *s*-process

elements (e.g., Smith et al. 2000), this may be due to a smaller sample size, especially if inhomogeneous pollution only affected a small percentage of intermediate-metallicity stars; however, this could explain the few observations in the literature of stars with $[Fe/H] \sim -1.4$ and $[Ba/Fe] \sim 0$ (e.g., Smith et al. 1995).

5.3.3. *The Metal-Rich Population*

For stars more metal-rich than $[Fe/H] \sim -1$, there is some evidence of a decrease in $[\alpha/Fe]$ and an increase in [Cu/Fe] (Pancino et al. 2002; but see also Cunha et al. 2002), which, if true, likely indicates an increased contribution from Type Ia SNe. Similarly, there appears to be a decrease in [Eu/Fe] with perhaps a similar decrease in the abundance of *s*-process elements relative to Fe (Norris & Da Costa; Smith et al. 2000). Although the Al data are rather incomplete in this metallicity regime, the general trends seen in slightly more metal-poor stars appear to continue.

While the scope of an age spread among the various metallicity populations is still unknown, the Al data presented here seem to indicate that the age difference between the intermediate and metal-rich populations is not especially large. In particular, stars with the largest values of $\log \epsilon(Al)$ appear with [Fe/H] ranging from -1.5 to -0.7, perhaps indicating that they formed from gas polluted by the same generation of IM-AGB ejecta. In this scenario, the lower [Al/Fe] ratios at high-metallicity might be due to those stars forming in regions where [Fe/H] increased due to inhomogeneous pollution by Type Ia SNe, as mentioned in Marcolini et al. (2007). In their scenario, this effect should be more important for the inner regions of the cluster. This may be corroborated by our finding that there is no apparent relationship between $\log \epsilon(Al)$ and distance from the cluster center, but a trend might be present for Fe such that stars with $[Fe/H] > -1$ are preferentially located closer to the cluster center. In any case, additional data are required in this metallicity regime to determine whether the decreasing [Al/Fe] ratios are a real effect or the result of incomplete statistics. It will be interesting to see if O and Na display similar behavior to Al as a function of [Fe/H].

6. SUMMARY

We have determined radial velocities, Fe, and Al abundances for 180 RGB stars in the Galactic globular cluster ω Cen using moderate resolution ($R \approx 13{,}000$) spectroscopy. The bulk of our sample includes stars with $V < 14.0$, but an observational bias is present such that we preferentially observed more luminous and more metal-poor stars. The spectra ranged from 6500–6750 Å and Fe abundances were based on an average of approximately 10–20 Fe I lines. Al abundances were determined using either spectrum synthesis or equivalent width analyses of the Al I $\lambda\lambda$6696, 6698 doublet, with synthesis being reserved for CN-strong and/or metal-rich stars.

With respect to our determined Fe abundances, we find in agreement with previous studies that at least four or more different metallicity populations are present in the cluster. Peaks in the metallicity distribution function appear at $[Fe/H] = -1.75$, -1.45, -1.05, and -0.75, indicating the presence of multiple star formation episodes. We do not find evidence suggesting any of the different metallicity populations are kinematically or spatially unique, but it should be noted that our observed completion fraction is low for stars more metal-rich than $[Fe/H] \sim -1.0$ and we only observed stars between about $2'$ and $20'$ from the cluster center.

Our Al data corroborate the Fe results such that there does not appear to be any correlation between Al abundance and distance from the cluster center or radial velocity. This suggests that the cluster gas was not significantly mixed while star formation was still occurring. In a plot of [Al/Fe] versus [Fe/H], the data reveal a star-to-star variation of nearly 1.3 dex that stays mostly constant until $[Fe/H] \sim -1.45$, in which case the spread in [Al/Fe] declines monotonically with increasing [Fe/H]. In addition, the [Al/Fe] floor remains nearly constant across all metallicities sampled here at $[Al/Fe] \sim +0.15$. This result is similar to what is predicted based on Type II SNe yields and closely mimics the trend seen in Galactic halo field stars. The anomalously low median [Al/Fe] ratio at $[Fe/H] = -1.45$ may be evidence for inhomogeneous pollution from Type Ia SNe and could explain the bimodal [Al/Fe] distribution seen in intermediate-metallicity stars, but more observations are required to confirm whether this is real or the result of an incomplete sample.

The source of the [Al/Fe] spread that has also been observed in other light elements remains an open problem, but the results obtained here pose some interesting questions. A plot of $\log \epsilon(Al)$ versus $\log \epsilon(Fe)$ shows that $\log \epsilon(Al)$ no longer increases beyond about 6.40 at metallicities higher than $[Fe/H] \sim -1.45$, which is coincident with the second peak in the metallicity distribution function. Apparently, whatever process is responsible for manifesting very high Al abundances shuts down or becomes less efficient at intermediate and high metallicities. In "normal" metal-poor globular clusters, the large star-to-star variations seen in the light elements are not shared by Fe-peak and neutron capture elements, and it has been suggested that HBB occurring in IM-AGB stars or in situ deep mixing are responsible for the light-element abundance anomalies. Without a comparable sample of O and Na data to supplement the Al abundances here, it is difficult to determine the role either source plays. However, AGB yields of stars undergoing HBB indicate stars forming from material polluted by AGB ejecta can only reach [Al/Fe] ratios between about +0.5 and +1.0, with perhaps slightly lower and higher values being reached in higher and lower metallicity environments, respectively.

It may be possible to explain the Al data such that core-collapse SNe drive the [Al/Fe] floor and an AGB mass spectrum with varying HBB efficiencies and mixing depths are responsible for much of the additional scatter present. The decrease in the maximum [Al/Fe] with increasing [Fe/H] might then be attributed to requiring higher mass stars for HBB to occur at temperatures adequate to activate the full ^{24}Mg to ^{27}Al cycle, which means the burning material is exposed for a shorter amount of time and thus leads to less [Al/Fe] enhancement. Whether this can be made to work quantitatively in light of the problems associated with AGB pollution scenarios (see § 1) remains to be seen.

We would like to thank the anonymous referee for a detailed and helpful report which improved the manuscript and for pointing out the possible significance of Type Ia SN pollution at intermediate metallicities. We would also like to thank Bob Kraft and Chris Sneden for helpful discussions regarding this paper and Bertrand Plez for providing an electronic copy of his CN line list. This publication makes use of data products from the Two Micron All Sky Survey, which is a joint project of the University of Massachusetts and the Infrared Processing and Analysis Center/California Institute of Technology, funded by the National Aeronautics and Space Administration and the

National Science Foundation. This research has made use of NASA's Astrophysics Data System Bibliographic Services. This research has made use of the SIMBAD database, operated at CDS, Strasbourg, France. Support for D. S. was provided by grant AST 01-39617 from the NSF for a summer REU program. Support of the College of Arts and Sciences and the Daniel Kirkwood fund at Indiana University Bloomington for C. I. J. is gratefully acknowledged.

Facilities: Blanco

REFERENCES

Alonso, A., Arribas, S., & Martinez-Roger, C. 1994, A&A, 282, 684
———. 1998, A&AS, 131, 209
———. 1999, A&AS, 140, 261
———. 2001, A&A, 376, 1039
Anders, E., & Grevesse, N. 1989, Geochim. Cosmochim. Acta, 53, 197
Anderson, J. 1997, Ph.D. thesis, Univ. California (Berkeley)
Arnett, W. D. 1971, ApJ, 166, 153
Arnett, W. D., & Truran, J. W. 1969, ApJ, 157, 339
Bedin, L. R., Piotto, G., Anderson, J., Cassisi, S., King, I. R., Momany, Y., & Carraro, G. 2004, ApJ, 605, L125
Bekki, K., & Norris, J. E. 2006, ApJ, 637, L109
Bell, R. A., Dickens, R. J., & Gustafsson, B. 1979, ApJ, 229, 604
Bellman, S., Briley, M. M., Smith, G. H., & Claver, C. F. 2001, PASP, 113, 326
Blackwell, D. E., & Shallis, M. J. 1977, MNRAS, 180, 177
Boesgaard, A. M., King, J. R., Cody, A. M., Stephens, A., & Deliyannis, C. P. 2005, ApJ, 629, 832
Briley, M. M., Cohen, J. G., & Stetson, P. B. 2004a, AJ, 127, 1579
Briley, M. M., Harbeck, D., Smith, G. H., & Grebel, E. K. 2004b, AJ, 127, 1588
Brown, J. A., & Wallerstein, G. 1993, AJ, 106, 133
Calamida, A., et al. 2005, ApJ, 634, L69
Cannon, R. D., Croke, B. F. W., Bell, R. A., Hesser, J. E., & Stathakis, R. A. 1998, MNRAS, 298, 601
Carbon, D. F., Romanishin, W., Langer, G. E., Butler, D., Kemper, E., Trefzger, C. F., Kraft, R. P., & Suntzeff, N. B. 1982, ApJS, 49, 207
Carpenter, J. M. 2001, AJ, 121, 2851
Castelli, F., Gratton, R. G., & Kurucz, R. L. 1997, A&A, 318, 841
Charbonnel, C., & Do Nascimento, J. D., Jr. 1998, A&A, 336, 915
Charbonnel, C., & Zahn, J.-P. 2007, A&A, 467, L15
Cohen, J. G., Briley, M. M., & Stetson, P. B. 2002, AJ, 123, 2525
Cohen, J. G., & Meléndez, J. 2005, AJ, 129, 303
Cunha, K., Smith, V. V., Suntzeff, N. B., Norris, J. E., Da Costa, G. S., & Plez, B. 2002, AJ, 124, 379
D'Antona, F., & Ventura, P. 2007, MNRAS, 379, 1431
Denisenkov, P. A., & Denisenkova, S. N. 1990, Soviet Astron. Lett., 16, 275
Denissenkov, P. A., & Herwig, F. 2003, ApJ, 590, L99
Denissenkov, P. A., & Weiss, A. 2001, ApJ, 559, L115
Dickens, R. J., Croke, B. F. W., Cannon, R. D., & Bell, R. A. 1991, Nature, 351, 212
Dinescu, D. I., Girard, T. M., & van Altena, W. F. 1999, AJ, 117, 1792
Djorgovski, S. 1993, in ASP Conf. Ser. Vol. 50, Structure and Dynamics of Globular Clusters, ed. S.G. Djorgovski & G. Meylan (San Francisco: ASP), 373
Fenner, Y., Campbell, S., Karakas, A. I., Lattanzio, J. C., & Gibson, B. K. 2004, MNRAS, 353, 789
Ferraro, F. R, Bellazzini, M., & Pancino, E. 2002, ApJ, 573, L95
Ferraro, F. R., Sollima, A., Pancino, E., Bellazzini, M., Straniero, O., Origlia, L., & Cool, A. M. 2004, ApJ, 603, L81
Fulbright, J. P. 2002, AJ, 123, 404
Gnedin, O. Y., Zhao, H., Pringle, J. E., Fall, S. M., Livio, M., & Meylan, G. 2002, ApJ, 568, L23
Gratton, R., Sneden, C., & Carretta, E. 2004, ARA&A, 42, 385
Gratton, R. G., Sneden, C., Carretta, E., & Bragaglia, A. 2000, A&A, 354, 169
Gratton, R. G., et al. 2001, A&A, 369, 87
Harris, W. E. 1996, AJ, 112, 1487
Hilker, M., Kayser, A., Richtler, T., & Willemsen, P. 2004, A&A, 422, L9
Hilker, M., & Richtler, T. 2000, A&A, 362, 895
Hill, V., et al. 2002, A&A, 387, 560
Hughes, J., & Wallerstein, G. 2000, AJ, 119, 1225
Hughes, J., Wallerstein, G., van Leeuwen, F., & Hilker, M. 2004, AJ, 127, 980
Ikuta, C., & Arimoto, N. 2000, A&A, 358, 535
Ivans, I. I., Kraft, R. P., Sneden, C., Smith, G. H., Rich, R. M., & Shetrone, M. 2001, AJ, 122, 1438
Ivans, I. I., Sneden, C., Kraft, R. P., Suntzeff, N. B., Smith, V. V., Langer, G. E., & Fulbright, J. P. 1999, AJ, 118, 1273
Johnson, C. I., Kraft, R. P., Pilachowski, C. A., Sneden, C., Ivans, I. I., & Benman, G. 2005, PASP, 117, 1308
Johnson, C. I., & Pilachowski, C. A. 2006, AJ, 132, 2346
Johnson, H. L. 1965, ApJ, 141, 923
Karakas, A., & Lattanzio, J. C. 2007, Publ. Astron. Soc. Australia, 24, 103
Kayser, A., Hilker, M., Richtler, T., & Willemsen, P. G. 2006, A&A, 458, 777
Keller, L. D., Pilachowski, C. A., & Sneden, C. 2001, AJ, 122, 2554
Kobayashi, C., Tsujimoto, T., Nomoto, K., Hachisu, I., & Kato, M. 1998, ApJ, 503, L155
Langer, G. E., Hoffman, R., & Sneden, C. 1993, PASP, 105, 301
Langer, G. E., Hoffman, R. E., & Zaidins, C. S. 1997, PASP, 109, 244
Langer, G. E., Kraft, R. P., Carbon, D. F., Friel, E., & Oke, J. B. 1986, PASP, 98, 473
Lattanzio, J., Karakas, A., Campbell, S., Elliott, L., & Chieffi, A. 2004, Mem. Soc. Astron. Italiana, 75, 322
Lee, Y.-W., Joo, J.-M., Sohn, Y.-J., Rey, S.-C., Lee, H.-C., & Walker, A. R. 1999, Nature, 402, 55
Lee, Y.-W., et al. 2005, ApJ, 621, L57
Maeder, A., & Meynet, G. 2006, A&A, 448, L37
Marcolini, A., Sollima, A., D'Ercole, A., Gibson, B. K., & Ferraro, F. R. 2007, MNRAS, 382, 443
Mayor, M., et al. 1997, AJ, 114, 1087
Merritt, D., Meylan, G., & Mayor, M. 1997, AJ, 114, 1074
Meylan, G., Mayor, M., Duquennoy, A., & Dubath, P. 1995, A&A, 303, 761
Norris, J. E. 2004, ApJ, 612, L25
Norris, J. E., & Da Costa, G. S. 1995, ApJ, 447, 680
Norris, J. E., Freeman, K. C., Mayor, M., & Seitzer, P. 1997, ApJ, 487, L187
Norris, J. E., Freeman, K. C., & Mighell, K. J. 1996, ApJ, 462, 241
Origlia, L., Ferraro, F. R., Bellazzini, M., & Pancino, E. 2003, ApJ, 591, 916
Pancino, E., Ferraro, F. R., Bellazzini, M., Piotto, G., & Zoccali, M. 2000, ApJ, 534, L83
Pancino, E., Galfo, A., Ferraro, F. R., & Bellazzini, M. 2007, ApJ, 661, L155
Pancino, E., Pasquini, L., Hill, V., Ferraro, F. R., & Bellazzini, M. 2002, ApJ, 568, L101
Pancino, E., Seleznev, A., Ferraro, F. R., Bellazzini, M., & Piotto, G. 2003, MNRAS, 345, 683
Pilachowski, C. A. 1988, ApJ, 326, L57
Pilachowski, C. A., Sneden, C., & Kraft, R. P. 1996, AJ, 111, 1689
Piotto, G., et al. 2005, ApJ, 621, 777
Platais, I., Wyse, R. F. G., Hebb, L., Lee, Y.-W., & Rey, S.-C. 2003, ApJ, 591, L127
Press, W. H., Teukolsky, S. A., Vetterling, W. T., & Flannery, B. R. 1992, Numerical Recipes in FORTRAN: The Art of Scientific Computing (2nd ed.; Cambridge: Cambridge Univ. Press)
Reijns, R. A., Seitzer, P., Arnold, R., Freeman, K. C., Ingerson, T., van den Bosch, R. C. E., van de Ven, G., & de Zeeuw, P. T. 2006, A&A, 445, 503
Rey, S.-C., Lee, Y.-W., Ree, C. H., Joo, J.-M., Sohn, Y.-J., & Walker, A. R. 2004, AJ, 127, 958
Richer, H. B., Fahlman, G. G., Buonanno, R., Fusi Pecci, F., Searle, L., & Thompson, I. B. 1991, ApJ, 381, 147
Ryan, S. G., Norris, J. E., & Beers, T. C. 1996, ApJ, 471, 254
Salaris, M., Cassisi, S., & Weiss, A. 2002, PASP, 114, 375
Samland, M. 1998, ApJ, 496, 155
Schaller, G., Schaerer, D., Meynet, G., & Maeder, A. 1992, A&AS, 96, 269
Shetrone, M. D. 1996, AJ, 112, 2639
Smith, G. H., Shetrone, M. D., Bell, R. A., Churchill, C. W., & Briley, M. M. 1996, AJ, 112, 1511
Smith, V. V., Cunha, K., Ivans, I. I., Lattanzio, J. C., Campbell, S., & Hinkle, K. H. 2005, ApJ, 633, 392
Smith, V. V., Cunha, K., & Lambert, D. L. 1995, AJ, 110, 2827
Smith, V. V., Suntzeff, N. B., Cunha, K., Gallino, R., Busso, M., Lambert, D. L., & Straniero, O. 2000, AJ, 119, 1239
Smith, V. V., Terndrup, D. M., & Suntzeff, N. B. 2002, ApJ, 579, 832
Sneden, C. 1973, ApJ, 184, 839
Sneden, C., Kraft, R. P., Guhathakurta, P., Peterson, R. C., & Fulbright, J. P. 2004, AJ, 127, 2162
Sneden, C., Kraft, R. P., Prosser, C. F., & Langer, G. E. 1991, AJ, 102, 2001
Sneden, C., Pilachowski, C. A., & Kraft, R. P. 2000, AJ, 120, 1351
Sollima, A., Borissova, J., Catelan, M., Smith, H. A., Minniti, D., Cacciari, C., & Ferraro, F. R. 2006, ApJ, 640, L43
Sollima, A., Ferraro, F. R., Pancino, E., & Bellazzini, M. 2005a, MNRAS, 357, 265
Sollima, A., Pancino, E., Ferraro, F. R., Bellazzini, M., Straniero, O., & Pasquini, L. 2005b, ApJ, 634, 332

Stanford, L. M., Da Costa, G. S., Norris, J. E., & Cannon, R. D. 2004, Mem. Soc. Astron. Italiana, 75, 290
———. 2006, ApJ, 647, 1075
———. 2007, ApJ, 667, 911
Suntzeff, N. B., & Kraft, R. P. 1996, AJ, 111, 1913
Thévenin, F. 1990, A&AS, 82, 179
Timmes, F. X., Woosley, S. E., & Weaver, T. A. 1995, ApJS, 98, 617
Tsujimoto, T., & Shigeyama, T. 2003, ApJ, 590, 803
van de Ven, G., van den Bosch, R. C. E., Verolme, E. K., & de Zeeuw, P. T. 2006, A&A, 445, 513
van Leeuwen, F., Le Poole, R. S., Reijns, R. A., Freeman, K. C., & de Zeeuw, P. T. 2000, A&A, 360, 472
van Loon, J. T., van Leeuwen, F., Smalley, B., Smith, A. W., Lyons, N. A., McDonald, I., & Boyer, M. L. 2007, MNRAS, 382, 1353
Ventura, P., & D'Antona, F. 2005a, A&A, 431, 279
———. 2005b, ApJ, 635, L149
———. 2008a, A&A, 479, 805
———. 2008b, MNRAS, 385, 2034
Villanova, S., et al. 2007, ApJ, 663, 296
Woolley, R. R. 1966, R. Obs. Ann., 2, 1
Woosley, S. E., & Weaver, T. A. 1995, ApJS, 101, 181
Yong, D., Grundahl, F., Lambert, D. L., Nissen, P. E., & Shetrone, M. D. 2003, A&A, 402, 985
Zucker, D., Wallerstein, G., & Brown, J. A. 1996, PASP, 108, 911